

# North Atlantic Holocene climate evolution recorded by high-resolution terrestrial and marine biomarker records

Moossen, Heiko; Bendle, James; Seki, Osamu; Quillmann, Ursula; Kawamura, Kimitaka

DOI:

[10.1016/j.quascirev.2015.10.013](https://doi.org/10.1016/j.quascirev.2015.10.013)

License:

Creative Commons: Attribution-NonCommercial-NoDerivs (CC BY-NC-ND)

*Document Version*

Peer reviewed version

*Citation for published version (Harvard):*

Moossen, H, Bendle, J, Seki, O, Quillmann, U & Kawamura, K 2015, 'North Atlantic Holocene climate evolution recorded by high-resolution terrestrial and marine biomarker records', *Quaternary Science Reviews*, vol. 129, pp. 111-127. <https://doi.org/10.1016/j.quascirev.2015.10.013>

[Link to publication on Research at Birmingham portal](#)

## **Publisher Rights Statement:**

After an embargo period this article is subject to the terms of a Creative Commons Attribution Non-Commercial No Derivatives license

Checked November 2015

## **General rights**

Unless a licence is specified above, all rights (including copyright and moral rights) in this document are retained by the authors and/or the copyright holders. The express permission of the copyright holder must be obtained for any use of this material other than for purposes permitted by law.

- Users may freely distribute the URL that is used to identify this publication.
- Users may download and/or print one copy of the publication from the University of Birmingham research portal for the purpose of private study or non-commercial research.
- User may use extracts from the document in line with the concept of 'fair dealing' under the Copyright, Designs and Patents Act 1988 (?)
- Users may not further distribute the material nor use it for the purposes of commercial gain.

Where a licence is displayed above, please note the terms and conditions of the licence govern your use of this document.

When citing, please reference the published version.

## **Take down policy**

While the University of Birmingham exercises care and attention in making items available there are rare occasions when an item has been uploaded in error or has been deemed to be commercially or otherwise sensitive.

If you believe that this is the case for this document, please contact [UBIRA@lists.bham.ac.uk](mailto:UBIRA@lists.bham.ac.uk) providing details and we will remove access to the work immediately and investigate.

**North Atlantic Holocene climate evolution recorded by high-resolution terrestrial and marine biomarker records.**

Heiko Moossen<sup>1\*</sup>, James Bendle<sup>1</sup>, Osamu Seki<sup>2</sup>, Ursula Quillmann<sup>3</sup>, Kimitaka Kawamura<sup>2</sup>,

<sup>1</sup> School of Geographical, Earth and Environmental Sciences; University of Birmingham; B15 2TT Birmingham; UK

<sup>2</sup> Institute of Low Temperature Science, Hokkaido University, N19W8, Kita-ku, 8 Sapporo, Hokkaido, 060-0819, Japan

<sup>3</sup> Institute of Arctic and Alpine Research, University of Colorado, 1560 30th Street, Boulder, CO 80309, USA

Key Words: Iceland, GDGT, alkenone; *n*-alkane; Holocene; climate reconstruction

**Please cite as:**

**Moossen, H., Bendle, J., Seki, O., Quillmann, U., Kawamura, K., 2015. North Atlantic Holocene climate evolution recorded by high-resolution terrestrial and marine biomarker records. Quaternary Science Reviews 129, 111-127.**

\* Corresponding Author; Tel: +44-(0)-121-4146139; e-mail: [h.moossen@bham.ac.uk](mailto:h.moossen@bham.ac.uk)

## Abstract

Holocene climatic change is driven by a plethora of forcing mechanisms acting on different time scales, including: insolation, internal ocean (e.g. Atlantic Meridional Overturning Circulation; AMOC) and atmospheric (e.g. North Atlantic Oscillation; NAO) variability. However, it is unclear how these driving mechanisms interact with each other. Here we present five, biomarker based, paleoclimate records (air-, sea surface temperature and precipitation), from a fjordic sediment core, revealing North Atlantic terrestrial and marine climate in unprecedented detail. The Early Holocene (10.7 - 7.8 kyrs BP) is characterised by relatively high air temperatures while SSTs are dampened by melt water events, and relatively low precipitation. The Middle Holocene (7.8 - 3.2 kyrs BP) is characterised by peak SSTs, declining air temperatures and high precipitation. A pronounced marine thermal maximum occurs between ~ 7 - 5.5 kyrs BP, 3000 years after the terrestrial thermal maximum, driven by melt water cessation and an accelerating AMOC. The neoglacal cooling, between 5.8 and 3.2 kyrs BP leads into the late Holocene. We demonstrate that an observed modern link between Icelandic precipitation variability during different NAO phases, may have existed from ~7.5 kyrs BP. A simultaneous decoupling of both air, and sea surface temperature records from declining insolation at ~3.2 kyrs BP may indicate a threshold, after which internal feedback mechanisms, namely the NAO evolved to be the primary drivers of Icelandic climate on centennial time-scales.

## 1. Introduction

A multitude of paleoclimate reconstructions show that the climate of the Holocene, the last ~11.5 kyrs (kilo years), has been far from stable (Bond et al., 2001; Mayewski et al., 2004; Wanner et al., 2011). Prominent climate events include the Holocene thermal maximum (HTM; Kaufman et al., 2004), the 8.2 event (Alley and Ágústsson, 2005), the neoglacial period (Jennings et al., 2002), the Medieval Climate Anomaly (MCA; Graham et al., 2011) and the Little Ice Age (LIA; Ogilvie and Jonsson, 2001). The latter climate events have had significant impacts on human societies (Buntgen et al., 2011; D'Andrea et al., 2011; deMenocal, 2001).

Holocene climatic change is attributed to a plethora of climatic drivers acting on different time scales (Mayewski et al., 2004; Wanner et al., 2011). The overarching external climate driver throughout the Holocene is the changing geometry of Earth's orbit around the sun, which over the last ~ 11 kyrs has driven decreasing summer insolation in the northern hemisphere (Laskar et al., 2004). This orbital cycle affects the climate on millennial and longer time scales by, for example, driving latitudinal shifts of the polar front and the Intertropical Convergence Zone (ITCZ; Haug et al., 2001; Knudsen et al., 2011). Superimposed on this lower-frequency orbital climate driver, higher-frequency volcanic activity and changes in the sun's intensity influence climate on annual to millennial timescales (Gray et al., 2010; Wanner et al., 2011). For example, the Maunder (solar) minimum contributed to the cooler climate of the LIA (Shindell et al., 2001), and recent models link solar activity with climate phenomena such as the North Atlantic Oscillation (Ineson et al., 2011).

The North Atlantic Oscillation (NAO) is the main driver of temperature and precipitation variability in the North Atlantic and Europe (Hurrell, 1995; Hurrell et al.,

2003). The NAO describes the strength and directional changes of the westerlies traversing the North Atlantic (Hurrell, 1995). When the NAO is in positive mode (NAO+), westerlies bring moist and warm air masses to Northern Europe (Fig. 1c), while southerly trending westerlies drive a drier and colder climate in Northern Europe when the NAO is in negative mode (NAO-; Hurrell et al., 2003; Fig. 1d). Contemporary observations indicate that the NAO operates over annual to decadal time scales (Hurrell, 1995; Hurrell et al., 2003). However, recent paleoclimate reconstructions show that atmospheric variations, attributed to NAO-type variability, have operated on centennial and even millennial time scales (Olsen et al., 2012; Trouet et al., 2009; Figs. 6h, i), contributing to prominent climatic events such as the MCA and the LIA (Trouet et al., 2009). Shifting NAO phases also influence the relative strength of the Irminger and North Icelandic Irminger Currents (IC and NIIC) in the Denmark Strait (Blindheim and Malmberg, 2005), whereby more warm, saline Atlantic Water flows through the Denmark Strait during NAO+, compared to NAO- phases (Figs. 1e, f).

The IC and NIIC are part of a network of currents contributing to the Atlantic Meridional Overturning Circulation (AMOC; Hansen and Østerhus, 2000; Vage et al., 2011). The AMOC mediates a significant amount of the pole-ward energy transfer in the northern Hemisphere and contributes to the current mild Northern European climate (Broecker, 1997). Changes in the intensity of the AMOC have been linked to changes in deep water production as indicated by velocity variations of Iceland Scotland Overflow Waters (Hall et al., 2004; Fig. 6k).

The solar, atmospheric and oceanic forcing mechanisms described above are some of the drivers that have been invoked to explain the climate evolution of the Holocene (Bond et al., 2001; Harrison et al., 1992; Mayewski et al., 2004). However, the

interactions of these climatic drivers, their relative importance, and the time scales on which they operate are still not well understood. This knowledge gap is evident when considering Bond cycles, which were first described nearly two decades ago (Bond et al., 1997; Fig. 6g). Bond cycles are defined as cyclical ( $\sim 1500 \pm 500$  years) penetrations of cold surface water, accompanied by drift ice, into the southeast North Atlantic (Bond et al., 1997). Such cycles are thought to be, at least in part, driven by changes in the sun's intensity (Bond et al., 2001). However, other driving mechanisms such as changes in the intensity of the AMOC, changing meridional atmospheric circulation, enhanced regional upwelling, changes in polar water fluxes and NAO indices have also been invoked as possible drivers of Bond cycles (Wanner et al., 2011; and references therein). Despite the number of driving mechanisms that are thought to cause Bond cycles, evidence of these events is not observed in all northern hemisphere paleoclimate records, and many paleoclimate records only show some, and not all of the Bond cycles (Wanner et al., 2011). For example, North Icelandic Shelf diatom and alkenone based sea surface temperature (SST) reconstructions do not show Bond cycles (Bendle and Rosell-Melé, 2007; Justwan et al., 2008; Fig. 6j), even though one might expect distinct N. Atlantic cold SST episodes to be recorded in Holocene sediments from the Icelandic margin.

Iceland and its surrounding waters have received significant scientific attention because climatic archives found in the area integrate proxy responses to most, if not all, climatic forcing mechanisms that have affected Holocene climate in the North Atlantic sector (Andrews and Jennings, 2014; Axford et al., 2011; Geirsdottir et al., 2002; Jennings et al., 2011; Quillmann et al., 2010; Quillmann et al., 2012). Consequently we present five new high-resolution paleoclimate records ( $n = 326$ ; 1 sample/ $\sim 30$  years; Figs. 6a - e) covering the period between  $\sim 10.7$  and  $\sim 0.3$  calibrated kilo years before

present (kyrs BP) from a single sediment core (MD99-2266) from Ísafjarðardjúp fjord in the Denmark Strait (Figs. 1a, b). Fjords are conducive to high sedimentation rates (Howe et al., 2010), facilitating high-resolution paleoclimate reconstructions. Moreover, since fjords bridge the land-ocean interface, paleo-environmental records from fjords provide a unique opportunity to study the link between marine and terrestrial climate. Our five new, biomarker based, reconstructions of three key climatic variables (SST, air temperature and precipitation) represent the most diverse array of marine and terrestrial, high-resolution paleoclimate signals extracted from a single marine archive thus far. The fact that all records are derived from a single sediment core allows their direct comparison without the potential bias inherent to different age models.

The multi-proxy approach is being facilitated by an expanding organic biomarker "toolbox" that enables paleoclimatologists to produce increasingly comprehensive climate reconstructions from a variety of climatic archives (Castañeda and Schouten, 2011; Eglinton and Eglinton, 2008). Here we use this approach to address the following question: to what extent and on what time scales have various climate forcing mechanisms influenced Icelandic SST, MAT and precipitation regimes?

## **2. Materials and Methods**

### **2.1. Core Location and Oceanography**

The Calypso piston core MD99-2266 was retrieved from the mouth of Ísafjarðardjúp fjord, Northwest Iceland (66° 13'77" N, 23° 15'93" W; Figs. 1a, b), from 106 m water depths, during Leg III of the 1999 IMAGES V cruise aboard the R/V *Marion Dufresne* (Quillmann et al., 2010 and references therein). It has a 10 cm diameter and a length of 3890 cm.

Ísafjarðardjúp fjord is the largest fjord of the Vestfirðir Peninsula. It is ~90 km long and 10 to 15 km wide. Together with its tributary fjords, it covers an area of ~1150 km<sup>2</sup> and drains ~2300 km<sup>2</sup> (Andrews et al., 2008). The Drangajökull icecap is located in the north eastern highlands of Vestfirðir Peninsula and its melt waters flow into Ísafjarðardjúp fjord and into Jökullfirðir, which is the largest tributary fjord of Ísafjarðardjúp (Andrews et al., 2008).

The core site is affected by two surface currents. The IC is the most westerly water current of the North Atlantic that brings warm Atlantic Water into the Nordic Seas. Today, the volume flux of the IC is estimated to be one Sverdrup (1 SV = 10<sup>6</sup> m<sup>3</sup> s<sup>-1</sup>) and its heat flux (relative to 0 °C) is estimated to be 25 Terra Watts (Hansen and Østerhus, 2000). The IC enters the Denmark Strait and divides into two branches. The NIIC branches off towards the east where it flows onto the North Icelandic Shelf. The second branch flows southwest along the Greenland coast, parallel to the East Greenland Current (EGC; Hansen and Østerhus, 2000). The Polar Front (PF) separates the warm and saline waters carried north by the IC from the colder and fresher polar waters which are carried south by the EGC (Jennings et al., 2011). The location of the PF is determined by the relative strengths of these warm and cold water currents (Ólafsdóttir et al., 2010).

## **2.2. Age model and Sampling Strategy**

The age model of MD99-2266 that was previously published by Quillmann et al. (2010) is used here. It consists of 24 <sup>14</sup>C-AMS (Accelerated Mass Spectrometry) dated bivalve and benthic foraminifera shells, as well as the Saksunarvatn tephra, which is located at a sediment depth of 3591 cm (Fig. 2). Quillmann *et al.* (2010) omitted 5 <sup>14</sup>C-AMS dates because the dates are older than the underlying dated horizons. Three of



those dates are in the top 23 cm suggesting that the core top sediments were disturbed (Quillmann et al., 2010). Quillmann et al. (2010) did not apply an ocean reservoir correction. The mean ( $2\sigma$  standard deviation) error associated with the 19  $^{14}\text{C}$ -dates that were used for the final age model, and the Saksunarvatn tephra layer, is  $\pm 165$  calibrated years. Following Moossen et al. (2013), sample ages were calculated assuming linear sedimentation rates (shown in Fig. 2) between each  $^{14}\text{C}$ -AMS dated sediment horizons and between the youngest  $^{14}\text{C}$ -AMS date and the core top.

Depending on the amount of available sediment, a minimum of  $1\text{ cm}^3$  and a maximum of  $6\text{ cm}^3$  of sediment were sampled from each time horizon. Where the piece of sediment representing a sample of a desired time interval was longer than 6 cm, an equal amount of sediment was taken from the beginning, the middle and the end of the sediment package representing one sample (time) interval. A total of 326 sediment samples were collected.

### **2.3. Sample preparation and analyses**

The methods for sample preparation and biomarker analyses are identical to the ones previously described by Moossen et al. (2013). Samples were solvent extracted using dichloromethane/methanol (3:1 v/v). An internal standard consisting of Squalane, 2-Nonadecanone, 1-Nonadecanol and Eruic acid was added to each sample. Samples were fractionated using silica gel column chromatography following Bendle et al. (2007).

A gas chromatograph (GC; Shimadzu 2010) with a flame ionisation detector (FID) and a Shimadzu OP2010-Plus Mass Spectrometer (MS) interfaced with a Shimadzu 2010 GC were used for the quantitative and qualitative analysis of alkenones and *n*-alkanes (Moossen et al., 2013). Compound separation was achieved using one of two identical columns, either a BP1 (SGE Analytical Science) or a TG-1MS (Thermo

Scientific) column (60m, diameter: 0.25 mm, film thickness: 0.25  $\mu\text{m}$ ; coating: 100 % Dimethyl-polysiloxane). The GC oven was held at 60  $^{\circ}\text{C}$  for two minutes, then the temperature was ramped up to 120  $^{\circ}\text{C}$  at 30  $^{\circ}\text{C min}^{-1}$  and then to 350  $^{\circ}\text{C}$  at 3  $^{\circ}\text{C min}^{-1}$ , where the temperature was held for 20 minutes. An injection standard consisting of methyl behenate was co-injected with each sample.

The relative tetraether abundances in 299 MD99-2266 sediment samples were analysed using high performance liquid chromatography-atmospheric pressure chemical ionisation-mass spectrometry (HPLC-APCI-MS) at the Organic Geochemistry Unit at the University of Bristol. Tetraether analysis was identical to that previously described in Moossen et al. (2013).

The hydrogen isotopic measurements of the  $\text{C}_{29}$ -*n*-alkane in 133 samples were conducted at the Institute of Low Temperature Science at the Hokkaido University, Japan. The isotopic values are expressed as per mil (‰; Eq. 1; vs. Standard Mean Ocean Water (SMOW)).

$$\delta(\text{‰}) = ((R_{\text{sample}} - R_{\text{standard}}) / R_{\text{standard}}) \times 1000 \quad \text{Eq. 1}$$

The hydrogen isotopic signature of the  $\text{C}_{29}$ -*n*-alkane ( $\delta\text{D}_{\text{C}_{29}}$ ) was analysed using an HP 6890 GC interfaced with a Finnigan MAT Delta Plus XL MS. The Finnigan MAT combustion furnace was held at 1450  $^{\circ}\text{C}$ . The chromatographic separation of the *n*-alkanes was accomplished using a DB5-HT column (Agilent J&W GC Columns; 30 m, 0.25 mm diameter; 0.1  $\mu\text{m}$  film thickness). The following GC oven temperature program was used: the temperature was ramped up from 50 to 120  $^{\circ}\text{C}$  at 10  $^{\circ}\text{C min}^{-1}$ , and then to 310  $^{\circ}\text{C}$  at 4  $^{\circ}\text{C min}^{-1}$ , where the temperature was held for 20 minutes. An external standard consisting of an *n*-alkane mix ( $\text{C}_{16}$  -  $\text{C}_{30}$ ) with a known hydrogen isotopic

composition was injected daily to evaluate the measurement drift of the instrument and ensure analytical precision. The isotopic composition of the C<sub>29</sub>-*n*-alkane and of the internal standard (Squalane) was calculated relative to the isotopic composition of an injection standard (Methyl Eicosanoate;  $\delta D$ : -226.8 ‰ vs SMOW) that was co-injected with each sample. The  $\delta D$  value of the internal standard squalane is  $-179.5 \pm 4.7$  ‰ (the uncertainty describes the  $1\sigma$  standard deviation (SD) of squalane in 133 samples over the entire time of analyses). 28 samples were analysed in duplicate and 2 in triplicate, and the  $1\sigma$  SD of the C<sub>29</sub>-*n*-alkane relative to the injection standard was  $\pm 3.5$  ‰. However, as not all samples were analysed in duplicate due to low *n*-alkane concentrations, we use the internal standard squalane that is present in all 299 samples to determine the analytical precision of the measurements.

## 2.4. Biomarker and statistical analyses

U<sup>K'</sup><sub>37</sub>-SSTs (Fig. 6a) were reconstructed from 326 samples using the relative abundance of the C<sub>37</sub>-alkenones with two (C<sub>37:2</sub>) and three (C<sub>37:3</sub>) double bonds. Relative abundances were converted into U<sup>K'</sup><sub>37</sub>-values after Prahl and Wakeham (1987; Eq. 2). The U<sup>K'</sup><sub>37</sub>-values were converted to SSTs using the calibration equation published by Conte et al. (2006; Eq. 3).

$$U_{37}^{K'} = C_{37:2}/(C_{37:2} + C_{37:3}) \quad \text{Eq. 2}$$

$$SST = (U_{37}^{K'} - 0.0709)/0.0322 \quad (\text{calibration error of } 1.1 \text{ }^{\circ}\text{C}) \quad \text{Eq. 3}$$

Thirty-four samples were analysed in triplicate and the mean analytical error ( $1\sigma$  SD) associated with the U<sup>K'</sup><sub>37</sub> index is  $\pm 0.01$  which translates into a temperature uncertainty of  $\pm 0.44$  °C.

The mean air temperatures (MATs) of 299 samples were reconstructed based on the relative abundance of branched glycerol-dialkyl-glycerol-tetraethers (br-GDGTs; Peterse et al., 2012; Weijers et al., 2007b). The cyclisation ratio (CBT, Eq. 4), and the methylation index of branched tetraethers (MBT', Eq. 5; Peterse et al., 2012) are converted to CBT/MBT'-MATs using the calibration equation published by Peterse et al. (2012; Eq. 6).

$$\text{CBT} = -\log ([\text{Ib} + \text{IIb}] / [\text{Ia} + \text{IIa}]) \quad \text{Eq. 4}$$

$$\text{MBT}' = ([\text{Ia} + \text{Ib} + \text{Ic}]) / ([\text{Ia} + \text{Ib} + \text{Ic}] + [\text{IIa} + \text{IIb} + \text{IIc}] + [\text{IIIa}]) \quad \text{Eq. 5}$$

$$\text{MAT} = 0.81 - 5.67 \times \text{CBT} + 31.0 \times \text{MBT}' \quad (\text{root mean square error of } 5^\circ\text{C}) \quad \text{Eq. 6}$$

The roman numerals in equations 3 and 4 refer to the relative abundance of the br-GDGT molecules (Fig. S3; SI 2). Nine samples were analysed in triplicate and two in duplicate and the  $1\sigma$  SD associated with the CBT/MBT'-MAT measurements is  $\pm 0.5^\circ\text{C}$ .

Soil pH variations were reconstructed using the revised calibration equation published by Peterse et al. (2012; Eq. 7).

$$\text{pH} = 7.90 - 1.97 \times \text{CBT} \quad (\text{root mean square error of } 0.8 \text{ pH units}) \quad \text{Eq. 7}$$

Nine samples were analysed in triplicate and two in duplicate and the  $1\sigma$  SD associated with the soil pH measurements is  $\pm 0.04$  pH units.

Following Moossen et al. (2013), Average chain length ( $\text{ACL}_{25-35}$ ) values from 310 samples were calculated using the concentrations of the most abundant odd-chained *n*-alkanes with 25 to 35 carbon atoms (Eq. 8; Schefuss et al., 2003). While Moossen et al. (2013) used the  $\text{ACL}_{25-35}$  record to identify 16 samples as outliers (see also Fig. S2; SI

2), the ACL<sub>25-35</sub> record, without the 16 outliers is published here and interpreted as showing precipitation change (see discussion below).

$$ACL_{25-35} = (\sum(X_i \times C_i)_n) / (C_i)_n \quad \text{Eq. 8}$$

$X_i$  represents the  $n$ -alkanes and  $C_i$  represents the abundance of the  $n$ -alkanes. 11 samples were analysed in triplicate and the mean  $1\sigma$  SD associated with the ACL<sub>25-35</sub> values is  $\pm 0.06$ .

The C<sub>29</sub>- $n$ -alkane was abundant enough for hydrogen isotopic analysis in 133 samples. The  $\delta D_{C29}$  values were corrected for the influence of the global ice volume on the hydrogen isotopic composition of meteoric water following Collins et al. (2013) and Niedermeyer et al. (2010) by using the benthic foraminifera oxygen isotope curve published by Waelbroeck et al. (2002; Fig. S1, SI 2). First, the uncorrected  $\delta D_{C29}$  value were converted to  $\delta^{18}O$  values using the meteoric water line equation published by Craig (1961). Then the  $\delta^{18}O$  value of each sample was corrected for the influence of ice volume using the 3rd order polynomial equation (Fig. S1, SI 2). Finally, the  $\delta^{18}O$  values of the samples were converted back into global ice volume corrected  $\delta D_{C29}$  values (Fig. 3).

REDFIT spectral analyses were conducted using PAST (Hammer et al., 2001; Fig. 7). REDFIT spectral analyses can be performed on unevenly spaced time series (Schulz and Mudelsee, 2002). This pre-empts the need for regular interpolation of the time series presented in this paper. An AR(1) red noise model and the 95 % confidence threshold is fitted to each spectral analyses.

### 3. Results and Discussion

#### 3.1. Paleoclimate proxies

The  $U^{K'}_{37}$ -SST proxy is based on variations of  $C_{37:2}$  and  $C_{37:3}$ -alkenones produced by certain haptophyte algae (e.g. *Emiliania huxleyi*) as a response to changing SSTs (Brassell et al., 1986). Previous studies have shown that the  $U^{K'}_{37}$ -index can be used to reconstruct SSTs on the Icelandic Shelf (Bendle and Rosell-Melé, 2007; Sicre et al., 2011). The  $U^{K'}_{37}$ -SSTs reported here tend to be higher than those reported previously on the North Icelandic Shelf (Bendle and Rosell-Melé, 2007; Sicre et al., 2011; Fig. 7h). Presumably this is due to the more southerly location of the Ísafjarðardjúp fjord with waters dominated by the warm IC and NIIC (Figs. 1e, f). Additionally,  $U^{K'}_{37}$ -SSTs are likely biased towards summer due to the predominant production of alkenones during summer months at high latitudes, as suggested for the Icelandic Shelf (Bendle and Rosell-Melé, 2007; Sicre et al., 2008b), the Southern Ocean (Sikes et al., 1997; Ternois et al., 1998) and the Gulf of Alaska (Prah et al., 2010). This is seemingly confirmed by the close match between core top and mean local summer June/July/August (JJA) SST of 9.6 °C at Stykkishólmur from 1867-1985 (Hanna et al., 2006; Fig. 6a). We assume that most of the sedimentary alkenones are produced locally and note that previous work demonstrates that potential mixing of allochthonous with *in situ* produced alkenones does not disturb the  $U^{K'}_{37}$ -SST relationship significantly on the Icelandic shelf (Bendle and Rosell-Melé, 2004).

Holocene  $U^{K'}_{37}$ -SSTs fluctuate between 6.6 °C at ~1.1 kyrs BP, and 14.8 °C at ~7.3 kyrs BP. The mean SST throughout the early Holocene is 10 °C. At the transition from the early to the middle Holocene, the amplitude of SST variability increases, and the onset of the middle Holocene sees the highest reconstructed SSTs (14.8 °C at ~7.3

kyrs BP). Between ~5.9 and ~3.2 kyrs BP SSTs decrease from 13.5 to 6.7 °C before rising again during the late Holocene. The mean SST during the late Holocene is 8.9 °C, but with significant variability around the mean throughout the last 2000 years of the record.

The CBT/MBT'-MAT reconstruction (Fig. 6b) is based on the variable abundances of br-GDGTs synthesised by subdivisions of *Acidobacteria* (Sinninghe Damsté et al., 2011) and other unspecified soil bacteria (Peterse et al., 2012; Weijers et al., 2007b). There is evidence that br-GDGTs are not amenable to aeolian transport (Gao et al., 2012), indicating that paleo proxies based on these compounds likely reflect a proximal Icelandic signal. The CBT/MBT'-MAT proxy is based on the assumption that br-GDGTs are exclusively produced by terrestrial organisms. Recent work suggests that br-GDGTs may have an aquatic source as well (Fietz et al., 2012), although direct evidence of such a source is still missing (Rueda et al., 2013). The CBT/MBT'-MATs in this study are mainly controlled by variations of just one br-GDGT compound. Throughout the Holocene, the relative concentration of br-GDGT IIIa increases from ~ 10 % to ~ 45 %, while the concentration of the other br-GDGTs remains relatively stable through time (SI 2; Fig. S4). The relative abundance of br-GDGT IIIa tracks changes of the previously published BIT-index closely (Fig. 4; Moossen et al., 2013). The BIT-index indicates changes in terrestrial soil input (Hopmans et al., 2004), and has been shown to yield reliable soil input results for Ísafjarðardjúp fjord (Moossen et al., 2013). This infers that GDGT IIIa is mainly derived from local Icelandic soils. Furthermore, previous studies have shown that the relative abundance of br-GDGT IIIa does not change significantly when comparing soils/near shore settings with open marine settings (Peterse et al., 2009; Zhu et al., 2011). These findings suggest that the primary climatic signals, CBT/MBT'-MAT, and also soil pH (see below), are preserved and not confounded by

any changes in terrestrial sediment, or marine vs. terrestrial source dynamics of Ísafjarðardjúp fjord and its catchment area.

Reconstructed CBT/MBT'-MATs follow decreasing Holocene summer insolation closely ( $r^2 = 0.84$ ; Fig. 5). Therefore we hypothesise that the primary control on CBT/MBT'-MAT is summer insolation change in this study. The close match between core top reconstructed temperatures and the mean instrumental summer air temperature (JJA) of 9.3 °C at Stykkishólmur from 1878-2002 (Fig. 6b; Hanna et al., 2004) seemingly supports the hypothesis that the CBT/MBT'-MATs represent summer season, rather than mean annual temperatures. Furthermore, the reconstructed CBT/MBT'-MATs of the most recent ~1.8 kyrs BP are in good agreement with reconstructed August air temperatures based on chironomid assemblages from north Iceland (Axford et al., 2009; Fig. 7). Finally, even though no clear evidence of a seasonal bias of the CBT/MBT'-MAT proxy has been found in soils at mid-latitudes (Weijers et al., 2011), studies conducted in the Skagerrak (58° N; Rueda et al., 2009) and in Arctic lakes (50° - 73°N; Shanahan et al., 2013) suggest that the CBT/MBT'-MAT proxy represents summer, rather than mean annual temperatures at high latitudes. Both, Rueda et al. (2009) and Shanahan et al. (2013) suggest that the bias towards summer season temperatures may be due to the br-GDGT producing soil bacteria being more active in the summer, when the soils are not frozen or snow covered. Since the calibration equation developed by Weijers et al. (2007b), and refined by Peterse et al. (2012) correlates br-GDGT variability with mean annual temperature (and no alternative summer-season CBT/MBT calibration is currently available), we continue to use CBT/MBT'-"MAT" in the text when referring to the br-GDGT air temperature changes, but we interpret the signal as weighted towards the summer, rather than mean annual temperatures.



The mean reconstructed Holocene CBT/MBT'-MAT is 11.8 °C. The highest CBT/MBT'-MAT of 16.6 °C is observed at 9.7 kyrs BP, and the lowest CBT/MBT'-MAT of 7.2 °C is observed at 540 yrs BP. The highest CBT/MBT'-MATs throughout the early Holocene are interrupted by a ~5 °C temperature drop between ~9.7 and ~9 kyrs BP. Subsequently MATs continually decrease from 16.5 °C at ~9 kyrs BP to 8.1 °C at ~3 kyr BP. Throughout the late Holocene, MATs fluctuate around a mean summer temperature of 9.5 °C.

Three independent qualitative approaches are presented here to estimate changes in precipitation. Firstly, we infer precipitation variability from soil pH changes that are reconstructed based on br-GDGTs variability (Peterse et al., 2012; Weijers et al., 2007b; Fig. 6c). Soil leaching processes result in soil acidification when precipitation is high (Johnson et al., 1998). The absolute soil pH values presented here suggest more alkaline soil types compared the dominant Icelandic soil type, andosol (Arnalds, 2008). Peterse et al. (2010) have shown that the br-GDGT proxy overestimates absolute soil pH values when applied to acidic soils, such as andosol (Arnalds, 2008). Therefore, we do not interpret absolute soil pH values, but rather temporal trends that are indicative of relative pH changes, driven by precipitation variability (Fawcett et al., 2011; Weijers et al., 2007a). As discussed previously, the br-GDGT based CBT/MBT'-MAT proxy likely records a summer season, rather than annual signal, possibly due to increased soil bacterial activity during the summer at high latitudes (Rueda et al., 2009; Shanahan et al., 2013). Consequently, it is likely that the br-GDGT based soil pH proxy also records a summer signal.

Secondly, we present two independent proxies based on higher plant wax derived *n*-alkanes that respond to precipitation change. *n*-Alkanes comprise part of the

protective wax layer that coats leaves (Eglinton et al., 1962). They are transported via aeolian and fluvial mechanisms into marine sediments and preserved over geological time periods (e.g. Eglinton and Eglinton, 2008, and references therein). Due to the proximity of the core location to land we suggest that the majority of the terrigenous material is derived from the catchment area of Ísafjarðardjúp fjord, likely transported during the spring melt following the winter snowfall maxima that is observed in modern Icelandic annual precipitation (Hanna et al., 2004).

The temporal variability of dominant (preferentially produced) leaf wax *n*-alkanes (ACL<sub>25-35</sub>) is controlled by: contributing plant types (e.g. Rommerskirchen et al., 2006b), ambient air temperature (Kawamura et al., 2003; Vogts et al., 2012) and precipitation regime (e.g. Calvo et al., 2004). The ACL<sub>25-35</sub> record presented here exhibits shifts of ~0.5 ACL<sub>25-35</sub> units at the transition from the early to the middle, and again from the middle to the late, and throughout the late Holocene (Fig. 6d). These shifts are remarkably large and occur over comparatively short time scales. Elsewhere, similar average chain length shifts have been associated with large scale changes from C<sub>3</sub> vegetation dominated landscapes to C<sub>4</sub> vegetation dominated landscapes (and vice versa) over glacial/interglacial time scales (Badewien et al., 2015; Calvo et al., 2004; Rommerskirchen et al., 2006a). Pollen studies from lake sediments and peat deposits show dynamic vegetation variability in Iceland throughout the Holocene. Vestfirðir peninsula vegetation was dominated by Cyperaceae (herbs) and Poaceae (grasses) with small amounts of *Salix*, *Juniperus* and *Betula* (birch) throughout the last 10,000 kyrs BP (Caseldine et al., 2003). *Betula* pollen first occurred between 7.8 and 7 kyrs BP but never increased above 20 % of the total land pollen sum throughout the pollen record (Caseldine et al., 2003). Elsewhere in northern Iceland birch woodland also became more abundant, until ca. 1000 yrs BP, when it declined again following the

settlement of Iceland (Hallsdottir, 1995). Trees produce more short chained *n*-alkanes than grasses (Rommerskirchen et al., 2006b; Vogts et al., 2009). Therefore, it is possible that an increase in the amount of *betula* pollen did contribute to the decreasing ACL<sub>25-35</sub> values between 7.8 and 7 kyrs BP. However, it is unlikely that the advent of the *betula* occurrence alone is responsible for the large shifts in ACL<sub>25-35</sub> throughout the record. Furthermore, pollen abundances from lake Vatnskotsvatn (northern Iceland) do not show major variations in the relative amounts of different types of plants (trees, grasses, herbs) between 3.2 and 1 kyr BP (Hallsdottir, 1995), during which time we observe large ACL<sub>25-35</sub> shifts (of an amplitude equivalent to that observed between 7.8 and 7 kyrs BP). Therefore, we suggest that changes in vegetation are not the main driver for ACL<sub>25-35</sub> shifts observed in MD99-2266 (Fig. 6d).

CBT/MBT'-MAT and ACL<sub>25-35</sub> co-vary throughout the late Holocene suggesting that temperature change may have influenced the leaf wax *n*-alkane distribution over the last 3000 yrs BP. However, no clear linear relationship between the CBT/MBT'-MAT and the ACL<sub>25-35</sub> records is observed for the entire Holocene ( $r^2 = 0.1$ ;  $n = 285$ ) suggesting that temperature is not the main driver for changes in the *n*-alkane distribution. While the linear correlation between the ACL<sub>25-35</sub> and soil pH records ( $r^2 = 0.2$ ;  $n = 285$ ) is only marginally stronger, the long term co variation of the ACL<sub>25-35</sub> and the soil pH record suggests that the ACL<sub>25-35</sub> responds to changes in precipitation. Assuming that leaf waxes are produced during the main growing season of plants at high latitudes, they likely record spring/summer, rather than annual precipitation.

The hydrogen isotopic composition of the C<sub>29</sub>-*n*-alkane ( $\delta D_{C29}$ ) is used as an additional proxy for precipitation change (Fig. 6e). The photosynthesis of organic matter by terrestrial higher plants utilizes soil water that ultimately derives from precipitation

(Sachse et al., 2012). The hydrogen isotopic compositions of leaf wax derived *n*-alkanes consequently reflect changes in precipitation and are an established proxy to reconstruct paleo-precipitation regimes (Sachse et al., 2012; Schefuss et al., 2005). The spatial and temporal isotopic variability of precipitation is controlled by hydrological variables, the continental, temperature and amount effects, and these need to be considered when interpreting the  $\delta D_{C29}$  isotopic signature (Sachse et al., 2012). For at least the last 1000 years, the amount of precipitation Iceland receives has been driven by the NAO (Hurrell, 1995; Trouet et al., 2009). Iceland receives more precipitation during NAO+, compared to NAO- phases (Hurrell, 1995). The close link between the NAO and precipitation amounts suggests that the main moisture source for Icelandic precipitation is the moisture transported by the westerly storm track that traverses the North Atlantic (Figs. 1c, d). While the latitudinal trajectory and the strength of these westerlies has decreased throughout the Holocene, their direction has remained the same (Harrison et al., 1992), suggesting that the hydrogen isotopic variability observed here cannot be attributed to major changes in water source areas. Therefore, we postulate that the  $\delta D_{C29}$  variability in the studied area reflects shifting NAO modes due to different precipitation regimes at least in the late Holocene. In the early Holocene, relatively high temperatures likely also influenced the isotopic signature of leaf wax components and will be discussed later.

The soil pH,  $ACL_{25-35}$  and  $\delta D_{C29}$  proxies all show remarkably similar millennial to centennial variability, particularly in the late Holocene (Figs. 6 and 7c, d, e). Therefore, we are confident that the interpretation of all three proxies in concert allows a robust interpretation of relative changes in precipitation.

The average proxy values spanning the Holocene are 7.9 for soil pH, 29.12 for  $ACL_{25-35}$ , and -197 ‰ for  $\delta D_{C29}$  (Figs. 6c, d, e). The combined precipitation proxy records tend towards less than average precipitation from ~10.7 to 7.8 kyrs BP, increased precipitation from ~7.8 to ~3 kyrs BP and considerable fluctuation around the mean throughout last 3 kyrs BP of the records.

### **3.2. Comparing terrestrial and marine biomarker records**

Magnetic susceptibility data from Ísafjarðardjúp and its tributary fjords shows that the post glacial sedimentation history has been very dynamic (Andrews et al., 2008). For example, high concentrations of magnetic minerals in early Holocene sediments reflect the final deglaciation of Iceland (Andrews et al., 2008). Such a dynamic sedimentation history has also been inferred through changing inputs of terrestrial vs. marine organic matter into Ísafjarðardjúp (Moossen et al., 2013). Moossen et al. (2013) argue that the build-up of soil and plant biomass in the aftermath of deglaciation, and subsequent soil erosion during the Neoglacial, and settlement of Iceland, led to a ~10 % increase in sedimentary terrestrial organic matter content in Ísafjarðardjúp from the early, through the middle, into the late Holocene. Dynamic erosion and sedimentation of terrestrial organic matter throughout the late Holocene has also been described in lake Haukadalur (Geirsdottir et al., 2009b), which lies just south of the Vestfirðir Peninsula. It is conceivable, as is the case in lake Haukadalur (Geirsdottir et al., 2009b), and in a Canadian fjord (Smittenberg et al., 2006), that increased sedimentation of terrestrial organic matter in the late Holocene, may have led to the deposition of a mix of fresh and old biomarkers. However, the comparison of the terrestrial biomarker data with other palaeoclimate records (see discussion below) clearly indicates that the biomarkers analysed in this study record climatic events. For example, the CBT/MBT'-MAT proxy follows declining insolation in the early, and middle Holocene. Additionally, when

comparing the five biomarker records to palaeo-NAO reconstructions (Olsen et al., 2012; Trouet et al., 2009) the records collectively show a synchronous response (see discussion below). Thus, the palaeoclimate records presented here indicate that the influence of old/reworked organic carbon was not significant enough to confound primary climatic signals.

Many of the conclusions drawn from the five biomarker records presented in this paper are based on the assumption that the temporal offset between the production and sedimentation of the different biomarkers does not exceed the resolution of the biomarker records. The integral prerequisite to this assumption is that the time it takes for the studied biomarkers to be transported from their respective precursor organisms into the sediment is similar enough that the interpreted signals indeed reflect the same climate events. Even if lateral transport of a small portion of alkenones is assumed, alkenones still have the most direct transport pathway into marine sediments compared to terrestrially derived br-GDGTs (Gao et al., 2012), that are thought to be mainly transported via fluvial mechanisms, and higher plant wax *n*-alkanes, that are transported via aeolian and fluvial mechanisms (e.g. Eglinton and Eglinton, 2008, and references therein). Here too, the synchronous response of the five biomarker records to NAO variations in the late Holocene suggests that the transport times of different biomarkers to the sediment are at least similar enough to resolve centennial scale climatic changes.

#### **4. Holocene climate evolution**

The five combined paleoclimate records from Ísafjarðardjúp fjord reveal terrestrial and marine climate in unprecedented detail for a marine sediment core record covering the entire Holocene (Figs. 6a-e). The combination of proxy records allows the

placement of new constraints on the relative importance of different climatic drivers for Icelandic climate throughout the Holocene. Below we discuss how the climate of the early, middle and late Holocene was likely driven by the changing relative influence of large-scale climatic drivers.

Concerted inspection of the  $U^{K'}_{37}$ -SST, the CBT/MBT'-MAT, and the precipitation records highlight two noteworthy and distinct climatic shifts at  $\sim 7.8$  and  $\sim 3.2$  kyrs BP (Fig. 6). No one individual proxy record clearly delimits these phase shifts, which is expected as individual proxies are recording marine or terrestrial temperatures or precipitation. These climatic parameters inherently have differential responses and sensitivity to external drivers and internal climate forcing mechanisms. Even in the case of the three proxies which record precipitation, different biogeochemical (biosynthesis of lipids) and physical processes (isotopic fractionation) are involved in transcribing the climatic signal, with a varying degrees of fidelity.

In the following section we will discuss the competing driving mechanisms that likely drove the climatic shifts at  $\sim 7.8$  and  $\sim 3.2$  kyrs BP. We explore the changing relative importance of the climate drivers, as they shaped the three distinct climatic periods of the Holocene.

#### **4.1. Early Holocene and glacial aftermath (10.7 to 7.8 kyrs BP)**

The CBT/MBT'-MAT reconstruction indicates that Icelandic terrestrial air temperatures were considerably warmer during the early Holocene than at any other time covered by the record (Fig. 6b). This observation is synchronous with a maxima in high northern hemisphere summer insolation (Laskar et al., 2004). Indeed, it is the close correlation between the reconstructed CBT/MBT'-MATs and summer insolation throughout the early and the middle Holocene, which indicates that summer insolation

was the main driver for summer season terrestrial climate (Fig. 5). The CBT/MBT'-MAT record also reveals that the terrestrial Holocene thermal maximum occurred between ~10.5 and ~8.5 kyrs BP. This timing broadly agrees with chironomide based temperature reconstructions, which indicate a terrestrial warm period between ~10.5 and 7.5 kyrs BP (Caseldine et al., 2003; Langdon et al., 2010). Increased primary production in lake Hvítárvatn also indicate warm summers between 10.2 and 9 kyrs BP (Larsen et al., 2012). Interestingly, there is no clear 8.2 kyr signal in the climate records presented here, compared to the GISP 2 oxygen isotope record (Grootes and Stuiver, 1997; Fig. 6i). The CBT/MBT'-MAT does drop during the period coinciding with the 8.2 kyr event, but the decrease is not significant when viewed in context of the early (and entire) Holocene record (Fig. 6b). Our sample resolution (27 samples between 8 - 8.4 kyrs BP: 1 sample/~15 yrs BP), is sufficient to capture the 8.2 kyr event, which lasted for ca. 400 years (Alley and Ágústsdóttir, 2005). However, there is only one data point within the period of the 8.2 kyr event that shows a noteworthy CBT/MBT'-MAT decrease. This suggests that either a) the 8.2 kyr event did not exert a significant influence on Icelandic terrestrial climate, or b) the CBT/MBT'-MAT proxy does not record it. The latter explanation is most likely, given that, numerous records suggest a significant impact of the 8.2 kyr event on climate in the North Atlantic sector (Alley and Ágústsdóttir, 2005; Quillmann et al., 2012; Rohling and Palike, 2005). Rohling and Palike (2005) find evidence that paleoclimate proxies biased towards summer seasons, do not record the 8.2 kyr event clearly. This is consistent with the CBT/MBT'-MAT proxy that likely records summer, rather than mean annual temperature at high latitudes (see discussion above).

$U_{37}^{K'}$ -SSTs do not show a clear relationship with insolation during the early Holocene (Fig. 6a). Indeed, while summer insolation peaked throughout the first 700



years of the Holocene, Icelandic  $U^{K'}_{37}$ -SSTs decreased by nearly 1.5 °C from ~10.7 to ~10 kyrs BP, before levelling out at ~9 °C for the next 900 years.  $\delta^{18}O$  analyses of foraminifera reveal that the IC started to influence the northern Denmark Strait 11 kyrs BP ago and was fully established by 10.2 kyrs BP (Ólafsdóttir et al., 2010). Reconstructed high marine paleoproductivity in Ísafjarðardjúp fjord during much of the early Holocene also points towards a penetration of nutrient rich Atlantic waters to the core site (Moossen et al., 2013). Despite the relatively warm Atlantic water transport of the IC, the occurrence of sea-ice indicating foraminifera and diatoms suggests that the Denmark Strait was also influenced by glacial melt water pulses, and/or repeated lateral shifts of the polar front (Andersen et al., 2004; Jennings et al., 2011). Benthic foraminiferal  $\delta^{18}O$  analyses from Ísafjarðardjúp fjord indicate that the coring site was influenced by glacial melt water throughout the early Holocene (Quillmann et al., 2010). Such melt water pulses can be attributed to a second, regional, climate driving mechanism: the residual melting of northern hemisphere ice sheets following the last glacial maximum. After the glacial advance throughout the Younger Dryas, the main ice sheet covering the Icelandic Highlands was retreating at 10.3 kyr BP (Geirsdóttir et al., 2009a), and the distal Greenland (Jennings et al., 2011), and Laurentide ice sheets (Alley and Ágústsdóttir, 2005) were also melting. Continual sea level rise suggests that land locked glaciers melted throughout the early, and into the middle Holocene until ~7 kyr BP (Siddall et al., 2010). Therefore, we attribute the dampened  $U^{K'}_{37}$ -SSTs, that are divergent from the CBT/MBT'-MAT trend and solar insolation, to the pervasive influence of glacial melt water in the early Holocene.

The early Holocene  $U^{K'}_{37}$ -SST record reveals two warm periods wherein SSTs rose by up to 2 °C, lasting from ~8.9 to ~8.5 kyrs BP and from ~8.1 to ~7.9 kyrs BP, that coincide with periods of high sunspot numbers (Solanki et al., 2004; Fig. 6f). Peak to

peak comparison of these intervals reveals that cooler background climate between ~8.5 and ~7.9 kyrs BP may have been driven by generally low sunspot numbers, with SST peaks coeval with transient spikes in solar activity. A similarly long (8.7 to 7.9 kyr BP) cool period is also evident from two lacustrine sites in central and north Iceland (Geirsdóttir et al., 2013; Larsen et al., 2012). The link between low sunspot numbers and low  $U_{37}^{K'}$ -SSTs is supported by Rohling and Palike (2005), who hypothesise that proxies reconstructing summer climate are driven by the suns activity. Modern Icelandic coastal waters feature an insolation induced thermocline during the summer months, resulting in a sharp temperature gradient from warmer surface waters to cooler deeper waters (Hanna et al., 2006). It seems likely that the Ísafjarðardjúp fjord water column was similarly, if not more stratified during the early Holocene when high summer insolation and glacial melt water events occurred. This mechanism could explain the coherence noted above between solar activity and the  $U_{37}^{K'}$ -SST proxy. We note that there is no discernible relationship between  $U_{37}^{K'}$ -SSTs and sun spot numbers elsewhere in the early Holocene, possibly due to internal mechanisms, e.g. melt water events causing colder SSTs and masking the effect of increased solar activity on the  $U_{37}^{K'}$ -SSTs.

The hypothesis that  $U_{37}^{K'}$ -SSTs are likely biased towards summer season temperatures may also explain the lack of a notable  $U_{37}^{K'}$ -SST drop during the 8.2 event, since Rohling and Palike (2005) suggest that summer season proxies do not sensitively record the 8.2 event. In contrast to the  $U_{37}^{K'}$ -SSTs, the  $\delta^{18}O$  record of benthic foraminifera from the same sediment core indicates a cooling and freshening of the IC at this time (Quillmann et al., 2012). Therefore, the biomarker and  $\delta^{18}O$  proxy records reveal a possible decoupling of surface photic zone summer temperatures from deeper

thermocline temperatures and increased stratification of the Denmark Strait water column during the early Holocene summer season.

All three precipitation records indicate that Iceland experienced a dryer than average summer climate during the early Holocene. Models indicate that the Icelandic low was located further north and stronger, than present, driving a stronger westerly jet, with increased precipitation and temperatures in winter (Harrison et al., 1992). The summer simulation of the same model suggests a reduced westerly jet during summer that would have led to a drier summer climate in north and central Europe (Harrison et al., 1992). Our precipitation proxies likely reflect summer, rather than winter precipitation (see discussion above), explaining their agreement with the modelled summer climate of the early Holocene. Not only the strength, but also the more northerly trajectory of the westerlies traversing the North Atlantic (Harrison et al., 1992; Knudsen et al., 2011) may have affected the precipitation regime. The proximity of the Greenland and Laurentide ice sheets may have contributed to the cooling of the westerlies causing them to hold less moisture and consequently resulting in a dryer Icelandic summer climate throughout the early Holocene. Finally, melt water induced cooling of regional SSTs may have contributed to lower precipitation: cold water evaporates less readily than warmer water, yielding relatively dryer maritime air masses, subsequently reduced precipitation on adjacent land masses.

The relatively high insolation and air temperatures coupled with the drier climate of the early Holocene would have caused relative increases in soil water evaporation and leaf water transpiration, leaving the available water for *n*-alkane biosynthesis depleted of the light isotope (Sachse et al., 2012). We argue that this depletion is reflected in the

high  $\delta D_{C29}$  values measured during the early Holocene, compared to the average Holocene conditions (Fig. 6e).

Interestingly, our record indicates that leaf wax isotopic values dropped by nearly 10 ‰ at the onset of the 8.2 kyr event and then recovered afterwards. None of the other climate proxies (both temperature and precipitation) show a significant response to the 8.2 kyr event. Models suggest the catastrophic influx of glacial melt-waters resulted in isotopically depleted surface waters in the North Atlantic region for decades after the initial event, regardless of the isotopic effects of any synchronous changes in temperature and precipitation (LeGrande and Schmidt, 2008). Thus in our record the transient changes to more negative isotope values at 8.2 kyr BP (and perhaps at 8.7 kyr BP) may reflect changes in the  $\delta D$  of the precipitation source, rather than local climate impacts or a change in precipitation source/pathway.

#### **4.2. Mid-Holocene and Neoglaciation (7.8 - 3.2 ka)**

At the transition from the early to the middle Holocene, while summer insolation and CBT/MBT'-MAT decreased, two rapid  $U^{K'}_{37}$ -SST warming events occurred (Fig. 6a). Centred on 7.6 and 7.3 kyr BP, both events lasted ~300 years, during which  $U^{K'}_{37}$ -SSTs spiked by ~5 °C (rising by a remarkable 0.5 °C per decade). Following the second event SSTs rose steadily over the next 1400 years by ~4 °C. These  $U^{K'}_{37}$ -SST peaks coincide with Bond cycles 5 and 4 (Fig. 6g). We term the period between 7.8 and 5.5 kyrs BP the 'marine Holocene thermal maximum (HTM)' as the highest  $U^{K'}_{37}$ -SSTs are observed during this interval. The marine HTM broadly coincides with diatom and coccolithophore based evidence for increased Atlantic water penetration onto the northwest Icelandic Shelf (Giraudeau et al., 2010; Justwan et al., 2008) and the highest SSTs observed off of south east Greenland (Jennings et al., 2011) and the North Icelandic Shelf (Justwan

et al., 2008; Fig. 6j) Furthermore, a major increase in reconstructed flow speed of the North Atlantic deep water across the Iceland-Scotland overflow ridge is centred on 7.2 kyr BP (Hall et al., 2004; Fig. 6k ). As regional components of the AMOC, deep-water flow speeds across the Iceland-Scotland ridge and the northward flow of warm surface currents in the Nordic Seas (including the Denmark Strait) are thought to be linked (Hall et al., 2004; Renssen et al., 2005), suggesting increased AMOC velocity acting as a contributing driver for the high  $U_{37}^{K'}$ -SSTs of the marine HTM.

The cessation of glacial melt water events at the transition from the early to middle Holocene affords a complimentary explanation for the marine HTM.  $\delta^{18}O$  signatures of *C. lobatulus* show that melt water pulses stopped affecting Ísafjarðardjúp waters from 7.9 kyr BP onwards (Quillmann et al., 2010). Intriguingly this coincides with the start of the first rapid  $U_{37}^{K'}$ -SST warming event noted above (Fig. 6a). This suggests that, once the dampening effect of glacial melt-water was removed, the still high (albeit decreasing) solar insolation, combined with a period of increased AMOC flow speed, drove a series of high SST episodes in Ísafjarðardjúp fjord.

The most striking observation when comparing the CBT/MBT'-MAT and  $U_{37}^{K'}$ -SST records is the temporal offset of ~3000 years between the maxima of the terrestrial HTM (~9.5 kyr BP) and the marine HTM (~6.5 kyr BP). Terrestrial and marine paleoclimate archives in the Iceland/Greenland region indicate that the HTM started at  $8.6 \pm 1.6$  kyrs, and ended at  $5.4 \pm 1.4$  kyrs (Kaufman et al., 2004). The uncertainties associated with the onset and end of the HTM may be due to the time it takes biologically based proxies to adjust to the HTM, i.e. the time it took *Betula* pollen to form mature vegetation and subsequently enough of a sedimentary pollen signature to be found in the paleoclimate record (Caseldine et al., 2003; Kaufman et al., 2004).

However, uncertainties in the timing of the HTM may also be due to the delayed response of specific parts of the environment to solar insolation as a climatic driver (Kaufman et al., 2004). One example is the spatial variability of the onset/termination of the HTM across the European/American Arctic sector. While the residual Laurentide ice sheet may have prevented the HTM from being expressed at sites surrounding the Hudson Bay, proxy records from Iceland were already influenced by the HTM (Kaufman et al., 2004).

In line with the latter explanation, we attribute the observed temporal discrepancy between the terrestrial and the marine HTM to the different responses of terrestrial and marine environments to solar radiation. Specifically, melt-water pulses dampened  $U_{37}^{K'}$ -SSTs during the early Holocene while CBT/MBT'-MATs were already driven by high insolation. Subsequently,  $U_{37}^{K'}$ -SSTs rose rapidly to form the marine HTM, 'delayed' by ~3000 years, but driven by declining, yet still high solar insolation, and possibly an accelerating AMOC.

We place the late Holocene neoglaciation between ~5.8 and ~3.2 kyrs BP, where both the  $U_{37}^{K'}$ -SST, and the CBT/MBT'-MAT records indicate decreasing temperatures in tandem with decreasing summer insolation. This corroborates observations from marine (Jennings et al., 2002; Justwan et al., 2008; Fig. 6j; Moros et al., 2006), and terrestrial records from Iceland (Geirsdóttir et al., 2013; Larsen et al., 2012; Moossen et al., 2013; Wastl et al., 2001). The neoglaciation culminated at ~3.2 kyrs BP with some of the lowest  $U_{37}^{K'}$ -SST and CBT/MBT'-MAT temperatures observed (Figs. 6a, b), coinciding with a global cool episode recognised in a number of records (Mayewski et al., 2004 and references therein). The late neoglacial decline in marine and terrestrial temperatures is clearly driven by declining insolation. However, an additional driver may

have been the decelerating AMOC (contributing to the  $U_{37}^K$ -SST decrease), culminating in the 2.7 ka event, as evidenced by declining Iceland Scotland overflow velocities (Hall et al., 2004; Fig. 6k).

The soil pH and  $ACL_{25-35}$  precipitation proxies (and to a lesser degree the  $\delta D_{C29}$  proxy) show a transition from less than average, to more than average precipitation at the onset of the middle Holocene (Figs. 6c,d,e) through to its termination ~3.2 kyr BP ago. Increasing precipitation throughout the middle Holocene is consistent with increased windiness/storms in Iceland and Greenland (Jackson et al., 2005; O'Brien et al., 1995), and with increased winter precipitation in western Norway (Bjune et al., 2005). The precipitation maxima throughout the middle Holocene may be explained by the large scale atmospheric shifts associated with declining summer insolation during this period (Knudsen et al., 2011). Specifically, the declining summer insolation gradient between the high and low latitudes (Laskar et al., 2004), caused a southward displacement of the ITCZ (Haug et al., 2001), the westerly jet across the North Atlantic and the mean position of the Icelandic low (Harrison et al., 1992). Our new precipitation data corroborates the scenario of Knudsen et al. (2011) that indicates that Iceland was situated directly in the path of the southwardly displaced, moisture carrying westerlies throughout the middle Holocene, and experienced high precipitation (Figs. 6c,d,e).

A clear correlation between increased precipitation in Iceland and NAO+ periods, has been observed in the instrumental record (Hanna et al., 2004; Hurrell, 1995). Proxy reconstructions of NAO variability now extend back through the MCA (Trouet et al., 2009), to 5.2 kyrs BP (Olsen et al., 2012). If the contemporary link between increased precipitation and NAO+ periods holds true throughout the Holocene, then our precipitation records suggest that a persistent NAO+ atmospheric pattern was prevalent

from at least 7.5 kyrs BP onwards, lasting until the end of the middle Holocene at 3.2 kyr BP. Evidence for increased storminess during the middle Holocene in Iceland (Jackson et al., 2005), along with a predominantly positive mode of the NAO, as reconstructed from Greenland lake redox states for much of the middle Holocene (Olsen et al., 2012) supports our hypothesis. Finally, the NAO may also have influenced North Atlantic SSTs during the middle Holocene (Andersen et al., 2004), however such variability is not obviously expressed in our  $U_{37}^{K'}$ -SST record.

#### **4.3. Late Holocene climate variability and the evolution of the modern NAO (3.2 - 0.3 ka)**

The late Holocene is the most socially relevant period in this study because of the clear and persistent influence climatic fluctuations had on human societies (Buntgen et al., 2011; D'Andrea et al., 2011; deMenocal, 2001). Our proxy records indicate that all climate parameters, precipitation, air-, and sea surface temperature underwent noteworthy change at the transition from the middle to the late Holocene (Figs. 6 and 7a, b, c, d, e).

From ~3.2 kyrs BP, the reconstructed CBT/MBT'-MAT and  $U_{37}^{K'}$ -SST temperature trends deviate from the continually decreasing summer insolation (Figs 6a, b). Intriguingly, the late Holocene is the only period where the CBT/MBT'-MAT reconstruction does not follow insolation change. The simultaneous decoupling of both CBT/MBT'-MAT and  $U_{37}^{K'}$ -SST records from insolation indicates a threshold, after which, a driving mechanism other than insolation started to dominate air and sea surface temperature variations over the most recent ~3.2 kyrs BP. Along with the temperature records, the soil pH precipitation record indicates a gradual, while the  $ACL_{25-35}$  and  $dD_{C29}$  records show a more abrupt precipitation decrease (Figs 6 and 7c, d, e). The periods from ~2.2 to ~1.3 kyrs BP, and from ~1.1 to ~0.5 kyrs BP are



characterised by relatively warm  $U_{37}^{K'}$ -SSTs, while CBT/MBT'-MATs tend to be cool, and precipitation tends to be elevated. Within  $^{14}\text{C}$ -AMS dating errors, these periods coincide with the Roman Warm Period (RWP), and the MCA (Geirsdóttir et al., 2013; Graham et al., 2011). In comparison, the periods from ~1.3 to ~1.1 kyrs BP, and from ~0.5 kyrs BP to ~0.3 kyrs BP, are characterised by cooler  $U_{37}^{K'}$ -SSTs, warmer CBT/MBT'-MATs, and lower precipitation. These periods coincide with the Dark Ages (DA; also known as the migration period; Buntgen et al., 2011; Sicre et al., 2008a) and the onset of the LIA (Ogilvie and Jonsson, 2001). In contrast with the asynchronous trends of precipitation, marine and terrestrial temperatures during the middle and early Holocene, all climate proxy records exhibit changes over four distinct climatic periods covering most of the late Holocene. This suggests one dominant controlling mechanism, most plausibly the NAO, which is known to affect sea surface temperature, air temperature and precipitation in Northern Europe and the North Atlantic sector (Hurrell, 1995; Hurrell et al., 2003). Assuming that the relationship between contemporary instrumental observations of precipitation, sea surface-, and air temperatures, and the NAO have remained constant throughout the late Holocene we would expect to observe the following climatic variations during positive NAO phases (compared to negative NAO phases): higher precipitation over Iceland (Hurrell, 1995; Hurrell et al., 2003; Figs. 1c, d), a higher throughput of warm Atlantic waters through the Denmark Strait, and therefore warmer SSTs (Blindheim and Malmberg, 2005; Figs. 1e, f). Higher air temperatures might also be expected, however, the link between air temperature and NAO is tenuous on Iceland (Hanna et al., 2004; Ólafsdóttir et al., 2013). The variability of the  $U_{37}^{K'}$ -SSTs and the precipitation records throughout the MCA and the LIA is in good agreement with reconstructed NAO variability (Olsen et al., 2012; Trouet et al.,

2009; Figs. 6h, i and 7f, g), lending credence to our hypothesis that NAO was the dominant forcing mechanism of Icelandic climate throughout the late Holocene.

Interestingly, Late Holocene centennial-scale CBT/MBT'-MAT variations are anti-phased with  $U_{37}^{K'}$ -SST throughout the RWP, DA, MCA and LIA (Figs. 6 and 7a, b). This would seemingly oppose contemporary (Hanna et al., 2004; Hurrell et al., 2003), and proxy based observations (Ólafsdóttir et al., 2013), of warmer air temperatures during NAO+ phases compared to NAO- phases. Specifically, the CBT/MBT'-MAT record indicates relatively low temperatures during the RWP and MCA (NAO+), compared to the higher reconstructed temperatures during the DA and LIA (NAO-). Additionally, the reconstructed CBT/MBT'-MAT temperatures are higher than the chironomid based August temperature reconstructed by Axford et al. (2009) during the DA and LIA, while the temperature records are in better agreement during the RWP and MCA. This suggests, that Icelandic CBT/MBT'-MAT temperature reconstructions provide temperature estimates that are too high during the periods characterised by NAO- periods. We hypothesise that this counterintuitive relationship between reconstructed CBT/MBT'-MAT and NAO mode is due to the proxies molecular variations that are mediated by soil bacteria, making the proxy a first order recorder of soil temperature change (Weijers et al., 2007b). Contemporary observations show that negative precipitation anomalies cause increased summer warmth throughout central Europe and are correlated to NAO fluctuations due to decreased latent cooling from soil moisture (Wang et al., 2011). Furthermore, dry soils warm more readily than wet soils (Al-Kayssi et al., 1990). Thus we hypothesise that during NAO- periods (LIA, DA), while precipitation was low (Fig. 6 and 7c, d, e), surface soils became relatively dry and were warmed more easily by solar radiation, compared to the relatively wet soils of NAO+ periods (MCA, RWP). Consequently, the counterintuitive centennial scale CBT/MBT'-

MAT trends during the Late Holocene may indicate soil temperature variations as a result of predominantly dry vs. predominantly wet soil conditions during the late Holocene. Following this hypothesis, the CBT/MBT'-MAT proxy may indirectly provide information on NAO variability via temperature dependency of the soil on changing precipitation regimes. This is supported by the correlated CBT/MBT'-MAT and precipitation records, demonstrating the advantage of considering multiple independent biomarker records in concert.

The argument, that all proxy records shown here are mainly affected by NAO fluctuations during the late Holocene, is supported by REDFIT spectral analyses conducted on the  $U^{K'}_{37}$ -SST, CBT/MBT'-MAT, soil pH, and the  $ACL_{25-35}$ -proxy records (Schulz and Mudelsee, 2002; Fig. 8). We note that the sampling resolution between ~2.1 and ~7.3 kyrs BP is not high enough to resolve the high frequency periodicities observed in the spectral analyses (SI 1). Therefore we limit the following interpretation to the late Holocene, from ~2.1 to ~0.3 kyrs BP where the sample resolution is 25 years/sample. All four records reveal periodicities between 64 and 96 years at the 95% significance level (Fig. 8). Such periodicities in instrumental records have been associated with the NAO (Rossi et al., 2011). Moreover, these periodicities have also been observed in the NAO reconstructions from Greenland lakes (Olsen et al., 2012), and in a varve-thickness record from Iceland (Ólafsdóttir et al., 2013). We note that the  $U^{K'}_{37}$ -SST and the CBT/MBT'-MAT temperature reconstructions also exhibit a significant spectral peak at ~130 years which, along with the spectral peaks between 64 and 96 years is associated with the Atlantic Meridional Oscillation (AMO; Knudsen et al., 2011; Rossi et al., 2011), that describes oscillatory variability of North Atlantic SSTs (Kerr, 2000; Schlesinger and Ramankutty, 1994). The influence of the AMO has also been postulated in the varve-thickness record from Iceland (Ólafsdóttir et al., 2013).

Therefore it is plausible that the AMO, alongside the NAO played a role in the late Holocene climate variations.

As discussed above, our biomarker proxies from MD99-2266 are likely weighted towards a spring/summer signal, rather than mean annual climate variability. However, the NAO is most prevalent during winter months (Hurrell, 1995; Hurrell and Deser, 2009). Thus we need to reconcile how biomarker proxies reconstructing summer climate can detect an atmospheric signal that is most prevalent during winter months. Hurrell and Deser (2009; and references therein) show that winter NAO indices can affect the climate of the following year by affecting slower components of the climate system (e.g. oceanic currents). Wang et al. (2011) show that European summer temperatures are highly correlated with the NAO regime of the previous year. Regionally, Blindheim and Malmberg (2005) have shown that changes of the winter sea level pressure gradients across the Denmark Strait are significantly correlated with SSTs of the following spring. Based on these observations in the instrumental record it seems plausible that the biomarker records presented here are influenced by changing NAO regimes, particularly when one considers that the sediment analysed for each data point throughout the late Holocene integrates between 10 and 25 years of climate.

We suggest insolation ceased to be a dominant driver of centennial scale climate events at the turn from the middle to the late Holocene. Instead, during this period of relatively low insolation, the climatic influence of internal feedback mechanisms, namely the NAO (and possibly the AMO) increasingly drove centennial scale changes, which are superimposed on the longer term, monotonic, insolation driven change. This suggests that lateral energy transport via warm surface currents and south-westerly winds became more important for Icelandic climate, rather than continually decreasing

insolation. This conclusion is supported by a varve thickness record from lake Hvítárvatn which indicates, that the NAO exerted increasing influence on Icelandic climate throughout the late Holocene (Ólafsdóttir et al., 2013).

## 5. Conclusions

The high-resolution, multi-proxy approach to climate reconstruction that is presented in this study gives a comprehensive picture of terrestrial and marine climate evolution throughout the Holocene. We show that major reorganisations of Holocene climate in Iceland took place at two climatic thresholds, one at ~7.8, and the other at ~3.2 kyrs BP. Based on the apparent changing importance of different climate drivers at ~7.3 and ~3.2 kyrs BP, we divide the Holocene into three distinct climatic periods, the early, middle and late Holocene. These climatic threshold events only become evident when considering the high-resolution terrestrial and marine biomarker proxy data in concert, illustrating the importance of the multi-proxy approach adopted here.

The combination of multiple biomarker proxies increases overall confidence in our interpretations and also reveals strengths and weaknesses of a particular proxy. For example, the confidence we have in the interpretation of soil pH,  $ACL_{25-35}$ , and  $\delta D_{C29}$  as recorders of precipitation is increased by the fact that all three records are in good agreement. Furthermore, the multi-proxy approach also reveals that the CBT/MBT'-MAT record may be significantly influenced by precipitation along with air temperature. The counterintuitive behaviour of the CBT/MBT'-MAT record in the late Holocene can be explained if the precipitation proxies are considered.

CBT/MBT'-MATs were mainly driven by high insolation causing the terrestrial HTM throughout the early Holocene (10.7 - 7.8 kyrs BP). In contrast,  $U^K_{37}$ -SSTs appear to be

dampened by the pervasive influence of glacial melt water events. Furthermore, the centennial variability in the  $U_{37}^{K'}$ -SST record illustrates the influence of solar activity, superimposed on the millennial scale melt water influence. The precipitation records indicate a dryer than average early Holocene summer climate, driven by: a reduced westerly jet during the summer months (Harrison et al., 1992) and reduced evaporation in source waters, due to the pervasive influence of melt water events.

The influence of melt water on the  $U_{37}^{K'}$ -SST record ceases at the transition of the early to the middle Holocene. Subsequently, an accelerating AMOC and decreasing, yet still high insolation drove a strong marine HTM that occurred ~3 kyrs after its terrestrial equivalent. The neoglacial period dominated the latter part of the middle Holocene and was driven by continually decreasing insolation, although the decelerating AMOC likely also affected  $U_{37}^{K'}$ -SSTs. Precipitation increased and remained high throughout the middle Holocene. The transition from a dryer to wetter than average climate is attributed to a decreasing summer insolation gradient that caused a southward shift of oceanic (AMO) and atmospheric (Iceland low and westerlies jet) circulation systems (Harrison et al., 1992; Knudsen et al., 2011). This shift placed Iceland under the direct influence of moisture carrying westerlies and drove the high precipitation regime of the middle Holocene.

All the paleoclimate records exhibit synchronous variability across four distinct climatic periods, the RWP, DA, MCA and LIA in the late Holocene. The comparison between of the precipitation,  $U_{37}^{K'}$ -SST and CBT/MBT'-MAT datasets presented here, and the NAO reconstructions by Trouet et al. (2009) and Olsen et al. (2012) indicates that the NAO became the dominant driver of Icelandic climate throughout the late Holocene. Furthermore, In conjunction with the NAO reconstruction of Olsen et al.

(2012), our data demonstrates that the observed link between increased precipitation in Iceland during NAO+ phases (Hurrell, 1995), that has previously been extended to the beginning of the MCA (Trouet et al., 2009), may have existed nearly from the onset of the middle Holocene at ~7.5 kyrs BP. Furthermore, assuming that NAO-type atmospheric fluctuations are the primary driver of high precipitation throughout the whole of the middle Holocene, our data indicates that the NAO was predominantly in a positive mode from ~ 7.8 to ~3.2 kyrs BP. If the amount of precipitation can be correlated with the strength of the westerlies ("strength" of the NAO), then our precipitation data shows that the westerlies (and possibly the NAO) were considerably stronger during the middle Holocene, compared to the late Holocene.

This study demonstrates that the interaction of different climate drivers drove the complex Holocene climate history. It agrees with findings of Larsen et al. (2012) and Geirsdóttir et al. (2013) who attribute the non-linear response of their palaeoclimate reconstructions to insolation to regional and local climate feedback mechanisms. In light of the fact that different climate drivers have shaped Icelandic climate throughout the early, middle and late Holocene, trying to ascribe pervasive climatic cycles spanning the entire Holocene (i.e. Bond cycles) to a single forcing mechanism would seemingly be futile. This conclusion offers one explanation as to why so many researchers have not been able to identify all, or even any Bond cycles in their Holocene records (Wanner et al., 2011).

## **6. Acknowledgements**

We thank an anonymous reviewer for the helpful and insightful comments. We thank the crew and staff of the *Marion Dufresne II*, and the CALYPSO coring team on the 1999 IMAGES cruise. We also thank Professor John Andrews for providing the core

material for this research, and the technical staff at the Institute of Arctic and Alpine Research. We thank Dr. Richard Pancost and technical staff at the Organic Geochemistry Unit, Bristol. We thank Dr. Ellen Roosen from the Woods Hole Oceanographic Institution who sent additional u-channels of the top most 3.5 meters of the sediment core archive half. We thank Dr. Fiona Meade for her help on Fig. 1 (<https://sites.google.com/site/meadescientificservices>). We thank the Scottish Alliance for Geoscience, Environment and Society (SAGES) who funded the PhD to Dr. Heiko Moossen. We thank the Japanese society for the promotion of science (JSPS) for funding a two months bursary to Dr. Heiko Moossen to Hokkaido University.

## 7. References

- Al-Kayssi, A.W., Al-Karaghoul, A.A., Hasson, A.M., Beker, S.A., 1990. Influence of Soil Moisture Content on Soil Temperature and Heat Storage under Greenhouse Conditions. *Journal of Agricultural Engineering Research* 45, 241-252.
- Alley, R.B., Ágústssdóttir, A.M., 2005. The 8k event: cause and consequences of a major Holocene abrupt climate change. *Quaternary Science Reviews* 24, 1123-1149.
- Andersen, C., Koc, N., Jennings, A., Andrews, J.T., 2004. Nonuniform response of the major surface currents in the Nordic Seas to insolation forcing: Implications for the Holocene climate variability. *Paleoceanography* 19.
- Andrews, J.T., Harðardóttir, J., Stoner, J.S., Principato, S.M., 2008. Holocene sediment magnetic properties along a transect from Isafiardardiup to Djupall, Northwest Iceland. *Arctic Antarctic and Alpine Research* 40, 1-14.
- Andrews, J.T., Jennings, A.E., 2014. Multidecadal to millennial marine climate oscillations across the Denmark Strait (similar to 66 degrees N) over the last 2000 cal yr BP. *Climate of the Past* 10, 325-343.
- Arnalds, O., 2008. Soils of Iceland. *Jokull* 58, 409-421.



941 Axford, Y., Andresen, C.S., Andrews, J.T., Belt, S.T., Geirsdóttir, Á., Massé, G., Miller,  
 942 G.H., Ólafsdóttir, S., Vare, L.L., 2011. Do paleoclimate proxies agree? A test comparing  
 943 19 late Holocene climate and sea-ice reconstructions from Icelandic marine and lake  
 944 sediments. *Journal of Quaternary Science* 26, 645-656.

945 Axford, Y., Geirsdóttir, Á., Miller, G., Langdon, P., 2009. Climate of the Little Ice Age and  
 946 the past 2000 years in northeast Iceland inferred from chironomids and other lake  
 947 sediment proxies. *Journal of Paleolimnology* 41, 7-24.

948 Badewien, T., Vogts, A., Dupont, L., Rullkötter, J., 2015. Influence of Late Pleistocene  
 949 and Holocene climate on vegetation distributions in southwest Africa elucidated from  
 950 sedimentary *n*-alkanes – Differences between 12°S and 20°S. *Quaternary Science*  
 951 *Reviews* 125, 160-171.

952 Bendle, J., Kawamura, K., Yamazaki, K., Niwai, T., 2007. Latitudinal distribution of  
 953 terrestrial lipid biomarkers and *n*-alkane compound-specific stable carbon isotope ratios  
 954 in the atmosphere over the western Pacific and Southern Ocean. *Geochimica Et*  
 955 *Cosmochimica Acta* 71, 5934-5955.

956 Bendle, J., Rosell-Melé, A., 2004. Distributions of  $U^{K}_{37}$  and  $U^{K'}_{37}$  in the surface waters  
 957 and sediments of the Nordic Seas: Implications for paleoceanography. *Geochemistry*  
 958 *Geophysics Geosystems* 5.

959 Bendle, J.A.P., Rosell-Melé, A., 2007. High-resolution alkenone sea surface temperature  
 960 variability on the North Icelandic Shelf: implications for Nordic Seas palaeoclimatic  
 961 development during the Holocene. *The Holocene* 17, 9-24.

962 Bjune, A.E., Bakke, J., Nesje, A., Birks, H.J.B., 2005. Holocene mean July temperature  
 963 and winter precipitation in western Norway inferred from palynological and glaciological  
 964 lake-sediment proxies. *The Holocene* 15, 177-189.

965 Blindheim, J., Malmberg, S.-A., 2005. The Mean Sea Level Pressure Gradient Across the  
 966 Denmark Strait as an Indicator of Conditions in the North Icelandic Irminger Current, In:  
 967 Drange, H., Dokken, T., Furevik, T., Gerdes, R., Berger, W. (Eds.), *The Nordic Seas: An*  
 968 *Integrated Perspective*. AGU, pp. 65-71.

969 Bond, G., Kromer, B., Beer, J., Muscheler, R., Evans, M.N., Showers, W., Hoffmann, S.,  
970 Lotti-Bond, R., Hajdas, I., Bonani, G., 2001. Persistent solar influence on North Atlantic  
971 climate during the Holocene. *Science* 294, 2130-2136.

972 Bond, G., Showers, W., Cheseby, M., Lotti, R., Almasi, P., deMenocal, P., Priore, P.,  
973 Cullen, H., Hajdas, I., Bonani, G., 1997. A pervasive millennial-scale cycle in North  
974 Atlantic Holocene and glacial climates. *Science* 278, 1257-1266.

975 Brassell, S.C., Eglinton, G., Marlowe, I.T., Pflaumann, U., Sarnthein, M., 1986. Molecular  
976 Stratigraphy - A new tool for climatic assessment. *Nature* 320, 129-133.

977 Broecker, W.S., 1997. Thermohaline Circulation, the Achilles Heel of Our Climate  
978 System: Will Man-Made CO<sub>2</sub> Upset the Current Balance? *Science* 278, 1582-1588.

979 Buntgen, U., Tegel, W., Nicolussi, K., McCormick, M., Frank, D., Trouet, V., Kaplan, J.O.,  
980 Herzig, F., Heussner, K.U., Wanner, H., Luterbacher, J., Esper, J., 2011. 2500 Years of  
981 European Climate Variability and Human Susceptibility. *Science* 331, 578-582.

982 Calvo, E., Pelejero, C., Logan, G.A., De Deckker, P., 2004. Dust-induced changes in  
983 phytoplankton composition in the Tasman Sea during the last four glacial cycles.  
984 *Paleoceanography* 19, 10.

985 Caseldine, C., Geirsdottir, A., Langdon, P., 2003. Efstadalsvatn - a multi-proxy study of a  
986 Holocene lacustrine sequence from NW Iceland. *Journal of Paleolimnology* 30, 55-73.

987 Castañeda, I.S., Schouten, S., 2011. A review of molecular organic proxies for examining  
988 modern and ancient lacustrine environments. *Quaternary Science Reviews* 30, 2851-  
989 2891.

990 Collins, J.A., Schefuß, E., Mulitza, S., Prange, M., Werner, M., Tharammal, T., Paul, A.,  
991 Wefer, G., 2013. Estimating the hydrogen isotopic composition of past precipitation using  
992 leaf-waxes from western Africa. *Quaternary Science Reviews* 65, 88-101.

993 Conte, M.H., Sicre, M.A., Rühlemann, C., Weber, J.C., Schulte, S., Schulz-Bull, D.,  
994 Blanz, T., 2006. Global temperature calibration of the alkenone unsaturation index (U<sup>K37</sup>)  
995 in surface waters and comparison with surface sediments. *Geochemistry Geophysics*  
996 *Geosystems* 7.

- 997 Craig, H., 1961. Isotopic Variations in Meteoric Waters. *Science* 133, 1702-1703.
- 998 D'Andrea, W.J., Huang, Y., Fritz, S.C., Anderson, N.J., 2011. Abrupt Holocene climate  
999 change as an important factor for human migration in West Greenland. *Proceedings of*  
1000 *the National Academy of Sciences of the United States of America* 108, 9765-9769.
- 1001 deMenocal, P.B., 2001. Cultural responses to climate change during the Late Holocene.  
1002 *Science* 292, 667-673.
- 1003 Eglinton, G., Gonzalez, A.G., Hamilton, R.J., Raphael, R.A., 1962. Hydrocarbon  
1004 constituents of the wax coatings of plant leaves: a taxonomic survey. *Phytochemistry* 1,  
1005 89 - 102.
- 1006 Eglinton, T.I., Eglinton, G., 2008. Molecular proxies for paleoclimatology. *Earth and*  
1007 *Planetary Science Letters* 275, 1-16.
- 1008 Fawcett, P.J., Werne, J.P., Anderson, R.S., Heikoop, J.M., Brown, E.T., Berke, M.A.,  
1009 Smith, S.J., Goff, F., Donohoo-Hurley, L., Cisneros-Dozal, L.M., Schouten, S., Sinninghe  
1010 Damste, J.S., Huang, Y., Toney, J., Fessenden, J., WoldeGabriel, G., Atudorei, V.,  
1011 Geissman, J.W., Allen, C.D., 2011. Extended megadroughts in the southwestern United  
1012 States during Pleistocene interglacials. *Nature* 470, 518-521.
- 1013 Fietz, S., Huguet, C., Bendle, J., Escala, M., Gallacher, C., Herfort, L., Jamieson, R.,  
1014 Martinez-Garcia, A., McClymont, E.L., Peck, V.L., Prahl, F.G., Rossi, S., Rueda, G.,  
1015 Sanson-Barrera, A., Rosell-Mele, A., 2012. Co-variation of crenarchaeol and branched  
1016 GDGTs in globally-distributed marine and freshwater sedimentary archives. *Global and*  
1017 *Planetary Change* 92-93, 275-285.
- 1018 Gao, L., Nie, J., Clemens, S., Liu, W., Sun, J., Zech, R., Huang, Y., 2012. The  
1019 importance of solar insolation on the temperature variations for the past 110 kyr on the  
1020 Chinese Loess Plateau. *Palaeogeography, Palaeoclimatology, Palaeoecology* 317–318,  
1021 128-133.
- 1022 Geirsdottir, A., Andrews, J.T., Olafsdottir, S., Helgadottir, G., Hardardottir, J., 2002. A 36  
1023 Ky record of iceberg rafting and sedimentation from north-west Iceland. *Polar Research*  
1024 21, 291-298.

- 1025 Geirsdottir, A., Miller, G.H., Axford, Y., Olafsdottir, S., 2009a. Holocene and latest  
1026 Pleistocene climate and glacier fluctuations in Iceland. *Quaternary Science Reviews* 28,  
1027 2107-2118.
- 1028 Geirsdóttir, Á., Miller, G.H., Larsen, D.J., Ólafsdóttir, S., 2013. Abrupt Holocene climate  
1029 transitions in the northern North Atlantic region recorded by synchronized lacustrine  
1030 records in Iceland. *Quaternary Science Reviews* 70, 48-62.
- 1031 Geirsdottir, A., Miller, G.H., Thordarson, T., Olafsdottir, K.B., 2009b. A 2000 year record  
1032 of climate variations reconstructed from Haukadalsvatn, West Iceland. *Journal of*  
1033 *Paleolimnology* 41, 95-115.
- 1034 Giraudeau, J., Grelaud, M., Solignac, S., Andrews, J.T., Moros, M., Jansen, E., 2010.  
1035 Millennial-scale variability in Atlantic water advection to the Nordic Seas derived from  
1036 Holocene coccolith concentration records. *Quaternary Science Reviews* 29, 1276-1287.
- 1037 Graham, N.E., Ammann, C.M., Fleitmann, D., Cobb, K.M., Luterbacher, J., 2011. Support  
1038 for global climate reorganization during the "Medieval Climate Anomaly". *Clim Dyn* 37,  
1039 1217-1245.
- 1040 Gray, L.J., Beer, J., Geller, M., Haigh, J.D., Lockwood, M., Matthes, K., Cubasch, U.,  
1041 Fleitmann, D., Harrison, G., Hood, L., Luterbacher, J., Meehl, G.A., Shindell, D., van  
1042 Geel, B., White, W., 2010. Solar influences on climate. *Rev. Geophys.* 48, 53.
- 1043 Gronvold, K., Oskarsson, N., Johnsen, S.J., Clausen, H.B., Hammer, C.U., Bond, G.,  
1044 Bard, E., 1995. Ash layers from iceland in the Greenland GRIP ice core correlated with  
1045 oceanic and land sediments. *Earth and Planetary Science Letters* 135, 149-155.
- 1046 Grootes, P.M., Stuiver, M., 1997. Oxygen 18/16 variability in Greenland snow and ice  
1047 with  $10^{-3}$ - $10^{-5}$  year time resolution. *J. Geophys. Res.* 102, 26455-26470.
- 1048 Hall, I.R., Bianchi, G.G., Evans, J.R., 2004. Centennial to millennial scale Holocene  
1049 climate-deep water linkage in the North Atlantic. *Quaternary Science Reviews* 23, 1529-  
1050 1536.
- 1051 Hallsdottir, M., 1995. On the pre-settlement history of Icelandic vegetation. *Buvisindi* 9,  
1052 17-29.

- 1053 Hammer, Ø., Harper, D.A.T., Ryan, P.D., 2001. PAST: Paleontological Statistics software  
1054 package for education and data analysis. *Palaeontologia Electronica* 4(1):9 pp., 2.17c ed.
- 1055 Hanna, E., Jonsson, T., Box, J.E., 2004. An analysis of Icelandic climate since the  
1056 nineteenth century. *International Journal of Climatology* 24, 1193-1210.
- 1057 Hanna, E., Jonsson, T., Olafsson, J., Valdimarsson, H., 2006. Icelandic coastal sea  
1058 surface temperature records constructed: Putting the pulse on air-sea-climate  
1059 interactions in the northern North Atlantic. Part I: Comparison with HadISST1 open-ocean  
1060 surface temperatures and preliminary analysis of long-term patterns and anomalies of  
1061 SSTs around Iceland. *Journal of Climate* 19, 5652-5666.
- 1062 Hansen, B., Østerhus, S., 2000. North Atlantic-Nordic Seas exchanges. *Progress In*  
1063 *Oceanography* 45, 109-208.
- 1064 Harrison, S.P., Prentice, I.C., Bartlein, P.J., 1992. Influence of insolation and glaciation  
1065 on atmospheric circulation in the North Atlantic sector: Implications of general circulation  
1066 model experiments for the Late Quaternary climatology of Europe. *Quaternary Science*  
1067 *Reviews* 11, 283-299.
- 1068 Haug, G.H., Hughen, K.A., Sigman, D.M., Peterson, L.C., Röhl, U., 2001. Southward  
1069 Migration of the Intertropical Convergence Zone through the Holocene. *Science* 293,  
1070 1304-1308.
- 1071 Hopmans, E.C., Weijers, J.W.H., Schefuss, E., Herfort, L., Damste, J.S.S., Schouten, S.,  
1072 2004. A novel proxy for terrestrial organic matter in sediments based on branched and  
1073 isoprenoid tetraether lipids. *Earth and Planetary Science Letters* 224, 107-116.
- 1074 Howe, J.A., Austin, W.E.N., Forwick, M., Paetzel, M., Harland, R., Cage, A.G., 2010.  
1075 Fjord systems and archives: a review. *Geological Society, London, Special Publications*  
1076 344, 5-15.
- 1077 Hurrell, J.W., 1995. Decadal trends in the North Atlantic Oscillation - Regional  
1078 temperatures and precipitation. *Science* 269, 676-679.
- 1079 Hurrell, J.W., Deser, C., 2009. North Atlantic climate variability: The role of the North  
1080 Atlantic Oscillation. *Journal of Marine Systems* 78, 28-41.

1081 Hurrell, J.W., Kushiner, Y., Ottersen, G., Visbeck, M., 2003. An overview of the North  
1082 Atlantic Oscillation. American Geophysical Union, Washington, DC, ETATS-UNIS.

1083 Ineson, S., Scaife, A.A., Knight, J.R., Manners, J.C., Dunstone, N.J., Gray, L.J., Haigh,  
1084 J.D., 2011. Solar forcing of winter climate variability in the Northern Hemisphere. *Nature*  
1085 *Geosci* 4, 753-757.

1086 Jackson, M.G., Oskarsson, N., Trønnnes, R.G., McManus, J.F., Oppo, D.W., Grönvold, K.,  
1087 Hart, S.R., Sachs, J.P., 2005. Holocene loess deposition in Iceland: Evidence for  
1088 millennial-scale atmosphere-ocean coupling in the North Atlantic. *Geology* 33, 509-512.

1089 Jennings, A., Andrews, J., Wilson, L., 2011. Holocene environmental evolution of the SE  
1090 Greenland Shelf North and South of the Denmark Strait: Irminger and East Greenland  
1091 current interactions. *Quaternary Science Reviews* 30, 980-998.

1092 Jennings, A.E., Knudsen, K.L., Hald, M., Hansen, C.V., Andrews, J.T., 2002. A mid-  
1093 Holocene shift in Arctic sea-ice variability on the East Greenland Shelf. *Holocene* 12, 49-  
1094 58.

1095 Johnson, D.W., Hanson, P.J., Todd, D.E., Susfalk, R.B., Trettin, C.F., 1998. Precipitation  
1096 Change and Soil Leaching: Field Results and Simulations from Walker Branch  
1097 Watershed, Tennessee. *Water, Air, & Soil Pollution* 105, 251-262.

1098 Justwan, A., Koç, N., Jennings, A.E., 2008. Evolution of the Irminger and East Icelandic  
1099 Current systems through the Holocene, revealed by diatom-based sea surface  
1100 temperature reconstructions. *Quaternary Science Reviews* 27, 1571-1582.

1101 Kaufman, D.S., Ager, T.A., Anderson, N.J., Anderson, P.M., Andrews, J.T., Bartlein, P.J.,  
1102 Brubaker, L.B., Coats, L.L., Cwynar, L.C., Duvall, M.L., Dyke, A.S., Edwards, M.E.,  
1103 Eisner, W.R., Gajewski, K., Geirsdóttir, A., Hu, F.S., Jennings, A.E., Kaplan, M.R.,  
1104 Kerwin, M.W., Lozhkin, A.V., MacDonald, G.M., Miller, G.H., Mock, C.J., Oswald, W.W.,  
1105 Otto-Bliesner, B.L., Porinchu, D.F., Rühland, K., Smol, J.P., Steig, E.J., Wolfe, B.B.,  
1106 2004. Holocene thermal maximum in the western Arctic (0-180°W). *Quaternary Science*  
1107 *Reviews* 23, 529-560.

- 1108 Kawamura, K., Ishimura, Y., Yamazaki, K., 2003. Four years' observations of terrestrial  
1109 lipid class compounds in marine aerosols from the western North Pacific. *Global*  
1110 *Biogeochem. Cycles* 17, 1003.
- 1111 Kerr, R.A., 2000. A North Atlantic climate pacemaker for the centuries. *Science* 288,  
1112 1984-1986.
- 1113 Knudsen, M.F., Seidenkrantz, M.-S., Jacobsen, B.H., Kuijpers, A., 2011. Tracking the  
1114 Atlantic Multidecadal Oscillation through the last 8,000 years. *Nature Communications* 2.
- 1115 Langdon, P.G., Leng, M.J., Holmes, N., Caseldine, C.J., 2010. Lacustrine evidence of  
1116 early-Holocene environmental change in northern Iceland: a multiproxy palaeoecology  
1117 and stable isotope study. *Holocene* 20, 205-214.
- 1118 Larsen, D.J., Miller, G.H., Geirsdóttir, Á., Ólafsdóttir, S., 2012. Non-linear Holocene  
1119 climate evolution in the North Atlantic: a high-resolution, multi-proxy record of glacier  
1120 activity and environmental change from Hvítárvatn, central Iceland. *Quaternary Science*  
1121 *Reviews* 39, 14-25.
- 1122 Laskar, J., Robutel, P., Joutel, F., Gastineau, M., Correia, A.C.M., Levrard, B., 2004. A  
1123 long-term numerical solution for the insolation quantities of the Earth. *Astronomy &*  
1124 *Astrophysics* 428, 261-285.
- 1125 LeGrande, A.N., Schmidt, G.A., 2008. Ensemble, water isotope-enabled, coupled general  
1126 circulation modeling insights into the 8.2 ka event. *Paleoceanography* 23.
- 1127 Mayewski, P.A., Rohling, E.E., Stager, J.C., Karlen, W., Maasch, K.A., Meeker, L.D.,  
1128 Meyerson, E.A., Gasse, F., van Kreveld, S., Holmgren, K., Lee-Thorp, J., Rosqvist, G.,  
1129 Rack, F., Staubwasser, M., Schneider, R.R., Steig, E.J., 2004. Holocene climate  
1130 variability. *Quaternary Research* 62, 243-255.
- 1131 Moossen, H., Abell, R., Quillmann, U., Bendle, J., 2013. Holocene changes in marine  
1132 productivity and terrestrial organic carbon inputs into an Icelandic fjord: Application of  
1133 molecular and bulk organic proxies. *The Holocene* 23, 11.

- 1134 Moros, M., Andrews, J.T., Eberl, D.D., Jansen, E., 2006. Holocene history of drift ice in  
1135 the northern North Atlantic: Evidence for different spatial and temporal modes.  
1136 *Paleoceanography* 21, PA2017.
- 1137 Niedermeyer, E.M., Schefuß, E., Sessions, A.L., Mulitza, S., Mollenhauer, G., Schulz, M.,  
1138 Wefer, G., 2010. Orbital- and millennial-scale changes in the hydrologic cycle and  
1139 vegetation in the western African Sahel: insights from individual plant wax  $\delta D$  and  $\delta^{13}C$ .  
1140 *Quaternary Science Reviews* 29, 2996-3005.
- 1141 O'Brien, S.R., Mayewski, P.A., Meeker, L.D., Meese, D.A., Twickler, M.S., Whitlow, S.I.,  
1142 1995. Complexity of Holocene climate as reconstructed from a Greenland ice core.  
1143 *Science* 270, 1962-1964.
- 1144 Ogilvie, A.E.J., Jonsson, T., 2001. "Little Ice Age" research: A perspective from Iceland.  
1145 *Climatic Change* 48, 9-52.
- 1146 Ólafsdóttir, K.B., Geirsdóttir, Á., Miller, G.H., Larsen, D.J., 2013. Evolution of NAO and  
1147 AMO strength and cyclicity derived from a 3-ka varve-thickness record from Iceland.  
1148 *Quaternary Science Reviews* 69, 142-154.
- 1149 Ólafsdóttir, S., Jennings, A.E., Geirsdóttir, Á., Andrews, J., Miller, G.H., 2010. Holocene  
1150 variability of the North Atlantic Irminger current on the south- and northwest shelf of  
1151 Iceland. *Marine Micropaleontology* 77, 101-118.
- 1152 Olsen, J., Anderson, N.J., Knudsen, M.F., 2012. Variability of the North Atlantic  
1153 Oscillation over the past 5,200 years. *Nature Geoscience* 5, 808-812.
- 1154 Peterse, F., Kim, J.-H., Schouten, S., Kristensen, D.K., Koç, N., Sinninghe Damsté, J.S.,  
1155 2009. Constraints on the application of the MBT/CBT palaeothermometer at high latitude  
1156 environments (Svalbard, Norway). *Organic Geochemistry* 40, 692-699.
- 1157 Peterse, F., Nicol, G.W., Schouten, S., Sinninghe Damsté, J.S., 2010. Influence of soil  
1158 pH on the abundance and distribution of core and intact polar lipid-derived branched  
1159 GDGTs in soil. *Organic Geochemistry* 41, 1171-1175.
- 1160 Peterse, F., van der Meer, J., Schouten, S., Weijers, J.W.H., Fierer, N., Jackson, R.B.,  
1161 Kim, J.-H., Sinninghe Damsté, J.S., 2012. Revised calibration of the MBT–CBT



1162 paleotemperature proxy based on branched tetraether membrane lipids in surface soils.  
1163 *Geochimica et Cosmochimica Acta* 96, 215-229.

1164 Prahl, F.G., Rontani, J.F., Zabeti, N., Walinsky, S.E., Sparrow, M.A., 2010. Systematic  
1165 pattern in U<sup>K37</sup> Temperature residuals for surface sediments from high latitude and other  
1166 oceanographic settings. *Geochimica Et Cosmochimica Acta* 74, 131-143.

1167 Prahl, F.G., Wakeham, S.G., 1987. Calibration of unsaturation patterns in long-chain  
1168 ketone compositions for paleotemperature assessment. *Nature* 330, 367-369.

1169 Quillmann, U., Jennings, A., Andrews, J., 2010. Reconstructing Holocene palaeoclimate  
1170 and palaeoceanography in Isafjaroardjup, northwest Iceland, from two fjord records  
1171 overprinted by relative sea-level and local hydrographic changes. *Journal of Quaternary*  
1172 *Science* 25, 1144-1159.

1173 Quillmann, U., Marchitto, T.M., Jennings, A.E., Andrews, J.T., Friestad, B.F., 2012.  
1174 Cooling and freshening at 8.2 ka on the NW Iceland Shelf recorded in paired  $\delta^{18}\text{O}$  and  
1175 Mg/Ca measurements of the benthic foraminifer *Cibicides lobatulus*. *Quaternary*  
1176 *Research* 78, 528-539.

1177 Renssen, H., Goosse, H., Fichefet, T., Brovkin, V., Driesschaert, E., Wolk, F., 2005.  
1178 Simulating the Holocene climate evolution at northern high latitudes using a coupled  
1179 atmosphere-sea ice-ocean-vegetation model. *Clim Dyn* 24, 23-43.

1180 Rohling, E.J., Palikey, H., 2005. Centennial-scale climate cooling with a sudden cold event  
1181 around 8,200 years ago. *Nature* 434, 975-979.

1182 Rommerskirchen, F., Eglinton, G., Dupont, L., Rullkötter, J., 2006a. Glacial/interglacial  
1183 changes in southern Africa: Compound-specific  $\delta^{13}\text{C}$  land plant biomarker and pollen  
1184 records from southeast Atlantic continental margin sediments. *Geochemistry,*  
1185 *Geophysics, Geosystems* 7, Q08010.

1186 Rommerskirchen, F., Plader, A., Eglinton, G., Chikaraishi, Y., Rullkötter, J., 2006b.  
1187 Chemotaxonomic significance of distribution and stable carbon isotopic composition of  
1188 long-chain alkanes and alkan-1-ols in C4 grass waxes. *Organic Geochemistry* 37, 1303-  
1189 1332.

- 1190 Rossi, A., Massei, N., Laignel, B., 2011. A synthesis of the time-scale variability of  
1191 commonly used climate indices using continuous wavelet transform. *Global and*  
1192 *Planetary Change* 78, 1-13.
- 1193 Rueda, G., Fietz, S., Rosell-Mele, A., 2013. Coupling of air and sea surface temperatures  
1194 in the eastern Fram Strait during the last 2000 years. *Holocene* 23, 692-698.
- 1195 Rueda, G., Rosell-Melé, A., Escala, M., Gyllencreutz, R., Backman, J., 2009. Comparison  
1196 of instrumental and GDGT-based estimates of sea surface and air temperatures from the  
1197 Skagerrak. *Organic Geochemistry* 40, 287-291.
- 1198 Sachse, D., Billault, I., Bowen, G.J., Chikaraishi, Y., Dawson, T.E., Feakins, S.J.,  
1199 Freeman, K.H., Magill, C.R., McInerney, F.A., van der Meer, M.T.J., Polissar, P., Robins,  
1200 R.J., Sachs, J.P., Schmidt, H.-L., Sessions, A.L., White, J.W.C., West, J.B., Kahmen, A.,  
1201 2012. Molecular Paleohydrology: Interpreting the Hydrogen-Isotopic Composition of Lipid  
1202 Biomarkers from Photosynthesizing Organisms. *Annual Review of Earth and Planetary*  
1203 *Sciences* 40, 221-249.
- 1204 Schefuss, E., Ratmeyer, V., Stuut, J.-B.W., Jansen, J.H.F., Sinninghe Damsté, J.S.,  
1205 2003. Carbon isotope analyses of n-alkanes in dust from the lower atmosphere over the  
1206 central eastern Atlantic. *Geochimica Et Cosmochimica Acta* 67, 1757-1767.
- 1207 Schefuss, E., Schouten, S., Schneider, R.R., 2005. Climatic controls on central African  
1208 hydrology during the past 20,000 years. *Nature* 437, 1003-1006.
- 1209 Schlesinger, M.E., Ramankutty, N., 1994. An oscillation in the global climate system of  
1210 period 65-70 years. *Nature* 367, 723-726.
- 1211 Schlitzer, R., 2010. Ocean Data View, <http://odv.awi.de>.
- 1212 Schulz, M., Mudelsee, M., 2002. REDFIT: estimating red-noise spectra directly from  
1213 unevenly spaced paleoclimatic time series. *Computers & Geosciences* 28, 421-426.
- 1214 Shanahan, T.M., Hughen, K.A., Van Mooy, B.A.S., 2013. Temperature sensitivity of  
1215 branched and isoprenoid GDGTs in Arctic lakes. *Organic Geochemistry* 64, 119-128.
- 1216 Shindell, D.T., Schmidt, G.A., Mann, M.E., Rind, D., Waple, A., 2001. Solar Forcing of  
1217 Regional Climate Change During the Maunder Minimum. *Science* 294, 2149-2152.

1218 Sicre, M.A., Hall, I.R., Mignot, J., Khodri, M., Ezat, U., Truong, M.X., Eiríksson, J.,  
1219 Knudsen, K.L., 2011. Sea surface temperature variability in the subpolar Atlantic over the  
1220 last two millennia. *Paleoceanography* 26, PA4218.

1221 Sicre, M.A., Jacob, J., Ezat, U., Rousse, S., Kissel, C., Yiou, P., Eiriksson, J., Knudsen,  
1222 K.L., Jansen, E., Turon, J.L., 2008a. Decadal variability of sea surface temperatures off  
1223 North Iceland over the last 2000 years. *Earth and Planetary Science Letters* 268, 137-  
1224 142.

1225 Sicre, M.A., Yiou, P., Eiriksson, J., Ezat, U., Guimbaut, E., Dahhaoui, I., Knudsen, K.L.,  
1226 Jansen, E., Turon, J.L., 2008b. A 4500-year reconstruction of sea surface temperature  
1227 variability at decadal time-scales off North Iceland. *Quaternary Science Reviews* 27,  
1228 2041-2047.

1229 Siddall, M., Abe-Ouchi, A., Andersen, M., Antonioli, F., Bamber, J., Bard, E., Clark, J.,  
1230 Clark, P., Deschamps, P., Dutton, A., Elliot, M., Gallup, C., Gomez, N., Gregory, J.,  
1231 Huybers, P., Kawarnura, K., Kelly, M., Lambeck, K., Lowell, T., Milrovica, J., Otto-  
1232 Bliesner, B., Richards, D., Stanford, J., Stirling, C., Stocker, T., Thomas, A., Thompson,  
1233 B., Toernqvist, T., Vazquez Riveiros, N., Waelbroeck, C., Yokoyama, Y., Yu, S., Grp,  
1234 P.L.W., 2010. The sea-level conundrum: case studies from palaeo-archives. *Journal of*  
1235 *Quaternary Science* 25, 19-25.

1236 Sikes, E.L., Volkman, J.K., Robertson, L.G., Pichon, J.-J., 1997. Alkenones and alkenes  
1237 in surface waters and sediments of the Southern Ocean: Implications for  
1238 paleotemperature estimation in polar regions. *Geochimica Et Cosmochimica Acta* 61,  
1239 1495-1505.

1240 Sinninghe Damsté, J.S., Rijpstra, W.I.C., Hopmans, E.C., Weijers, J.W.H., Foesel, B.U.,  
1241 Overmann, J., Dedysh, S.N., 2011. 13,16-Dimethyl Octacosanedioic Acid (iso-Diabolic  
1242 Acid), a Common Membrane-Spanning Lipid of Acidobacteria Subdivisions 1 and 3.  
1243 *Applied and Environmental Microbiology* 77, 4147-4154.

1244 Smittenberg, R.H., Eglinton, T.I., Schouten, S., Sinninghe Damsté, J.S., 2006. Ongoing  
1245 Buildup of Refractory Organic Carbon in Boreal Soils During the Holocene. *Science* 314,  
1246 1283-1286.

- 1247 Solanki, S.K., Usoskin, I.G., Kromer, B., Schussler, M., Beer, J., 2004. Unusual activity of  
1248 the Sun during recent decades compared to the previous 11,000 years. *Nature* 431,  
1249 1084-1087.
- 1250 Ternois, Y., Sicre, M.A., Boireau, A., Beaufort, L., Miquel, J.C., Jeandel, C., 1998.  
1251 Hydrocarbons, sterols and alkenones in sinking particles in the Indian Ocean sector of  
1252 the Southern Ocean. *Organic Geochemistry* 28, 489-501.
- 1253 Trouet, V., Esper, J., Graham, N.E., Baker, A., Scourse, J.D., Frank, D.C., 2009.  
1254 Persistent Positive North Atlantic Oscillation Mode Dominated the Medieval Climate  
1255 Anomaly. *Science* 324, 78-80.
- 1256 Vage, K., Pickart, R.S., Spall, M.A., Valdimarsson, H., Jonsson, S., Torres, D.J.,  
1257 Osterhus, S., Eldevik, T., 2011. Significant role of the North Icelandic Jet in the formation  
1258 of Denmark Strait overflow water. *Nature Geoscience* 4, 723-727.
- 1259 Vogts, A., Moossen, H., Rommerskirchen, F., Rullkotter, J., 2009. Distribution patterns  
1260 and stable carbon isotopic composition of alkanes and alkan-1-ols from plant waxes of  
1261 African rain forest and savanna C3 species. *Organic Geochemistry* 40, 1037-1054.
- 1262 Vogts, A., Schefuss, E., Badewien, T., Rullkötter, J., 2012. n-Alkane parameters from a  
1263 deep sea sediment transect off southwest Africa reflect continental vegetation and  
1264 climate conditions. *Organic Geochemistry* 47, 109-119.
- 1265 Waelbroeck, C., Labeyrie, L., Michel, E., Duplessy, J.C., McManus, J.F., Lambeck, K.,  
1266 Balbon, E., Labracherie, M., 2002. Sea-level and deep water temperature changes  
1267 derived from benthic foraminifera isotopic records. *Quaternary Science Reviews* 21, 295-  
1268 305.
- 1269 Wang, G., Dolman, A.J., Alessandri, A., 2011. A summer climate regime over Europe  
1270 modulated by the North Atlantic Oscillation. *Hydrology and Earth System Sciences* 15,  
1271 57-64.
- 1272 Wanner, H., Solomina, O., Grosjean, M., Ritz, S.P., Jetel, M., 2011. Structure and origin  
1273 of Holocene cold events. *Quaternary Science Reviews* 30, 3109-3123.

1274 Wastl, M., Stötter, J., Caseldine, C., 2001. Reconstruction of Holocene Variations of the  
1275 Upper Limit of Tree or Shrub Birch Growth in Northern Iceland Based on Evidence from  
1276 Vesturardalur-Skidadalur, Trölaskagi. *Arctic, Antarctic, and Alpine Research* 33, 191-203.

1277 Weijers, J.W.H., Bernhardt, B., Peterse, F., Werne, J.P., Dungait, J.A.J., Schouten, S.,  
1278 Sinninghe Damsté, J.S., 2011. Absence of seasonal patterns in MBT-CBT indices in mid-  
1279 latitude soils. *Geochimica Et Cosmochimica Acta* 75, 3179-3190.

1280 Weijers, J.W.H., Schefuss, E., Schouten, S., Sinninghe Damsté, J.S., 2007a. Coupled  
1281 thermal and hydrological evolution of tropical Africa over the last deglaciation. *Science*  
1282 315, 1701-1704.

1283 Weijers, J.W.H., Schouten, S., van den Donker, J.C., Hopmans, E.C., Sinninghe Damsté,  
1284 J.S., 2007b. Environmental controls on bacterial tetraether membrane lipid distribution in  
1285 soils. *Geochimica Et Cosmochimica Acta* 71, 703-713.

1286 Zhu, C., Weijers, J.W.H., Wagner, T., Pan, J.-M., Chen, J.-F., Pancost, R.D., 2011.  
1287 Sources and distributions of tetraether lipids in surface sediments across a large river-  
1288 dominated continental margin. *Organic Geochemistry* 42, 376-386.

1289

1290

1291

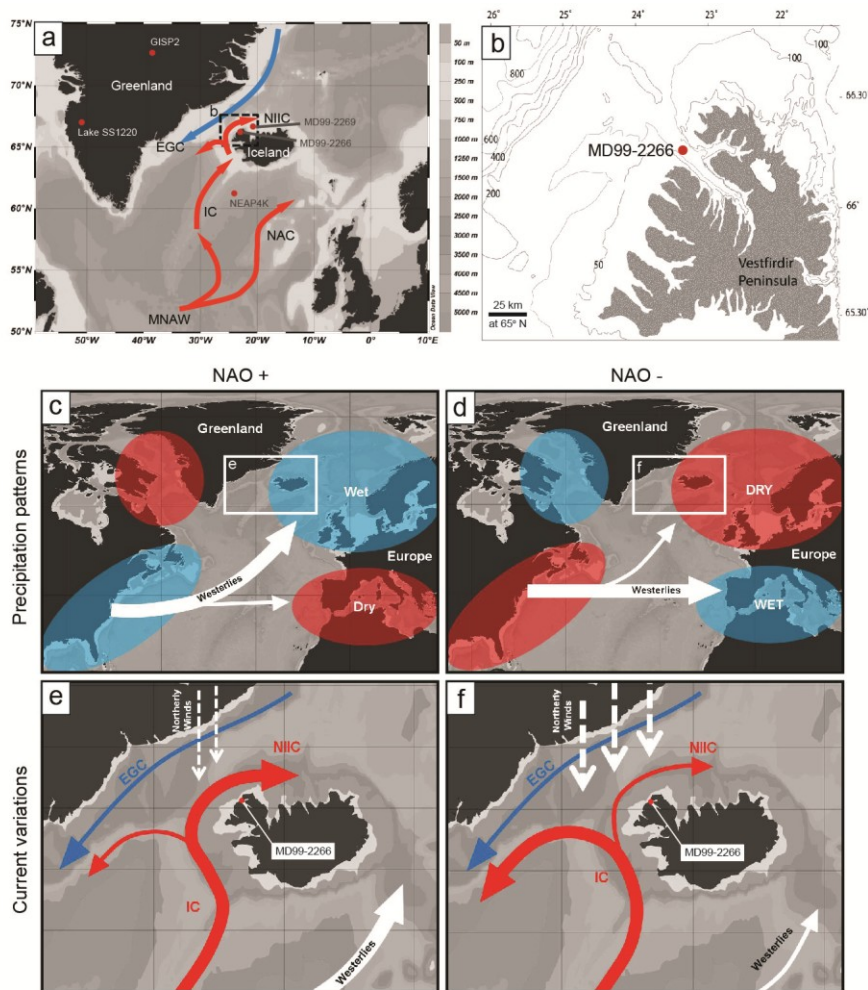


**Figure 1:** North Atlantic atmospheric and oceanic currents affecting the core (MD99-2266) location in the Denmark Strait. (a) Surface currents after Hansen and Østerhus (2000). Red arrows represent the Mean North Atlantic Water (MNAW) that branches into the North Atlantic Current (NAC) and the Irminger Current (IC). Part of the IC flows into the Denmark Strait and forms the North Icelandic Irminger Current (NIIC). The blue arrow represents the East Greenland Current (EGC). Core locations of compared datasets (Fig. 6), and of MD99-2266 are indicated by red dots. (b) Bathymetric map of Vestfirðir Peninsula with the core location (red dot) indicated in the mouth of Ísafjarðardjúp fjord. (c-f) Present day NAO influenced precipitation and current patterns. Iceland receives more precipitation during NAO+ (c), and less precipitation during NAO- (d) phases (Hurrell, 1995; precipitation patterns after: <http://www.ldeo.columbia.edu/res/pi/NAO>; Hurrell et al., 2003). NAO+ phases coincide with an increased Atlantic water influence on the North Icelandic Shelf and in the Denmark Strait, and decreased prevalence of northerly winds (e), and NAO- phases coincide with less Atlantic water influence in the Denmark Strait, and increased prevalence of northerly winds (f; Blindheim and Malmberg, 2005). Source of map: (Schlitzer, 2010).

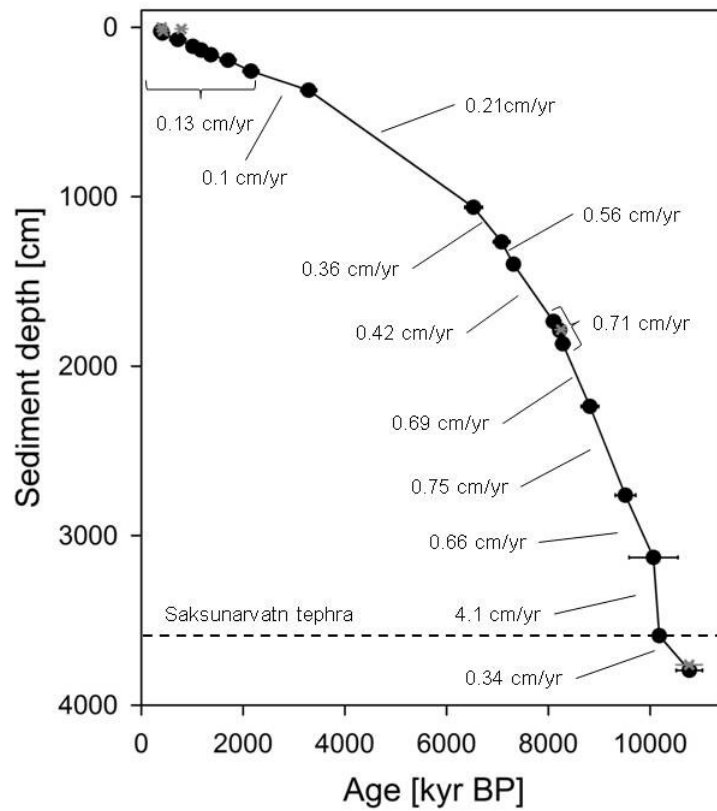


**Figure 2:** Age model of core MD99-2266 based on 19 (of a total of 24)  $^{14}\text{C}$ -AMS dated sediment horizons and the depth horizon of the Saksunarvatn tephra (dashed line) which is dated at  $10,180 \pm 120$  kyrs BP (Gronvold et al., 1995; Quillmann et al., 2010). The 5  $^{14}\text{C}$ -AMS dates discarded by Quillmann et al.(2010) are shown in grey. Sedimentation rates are calculated using the calibrated ages (kyr BP) of the dated horizons.

1294

1295

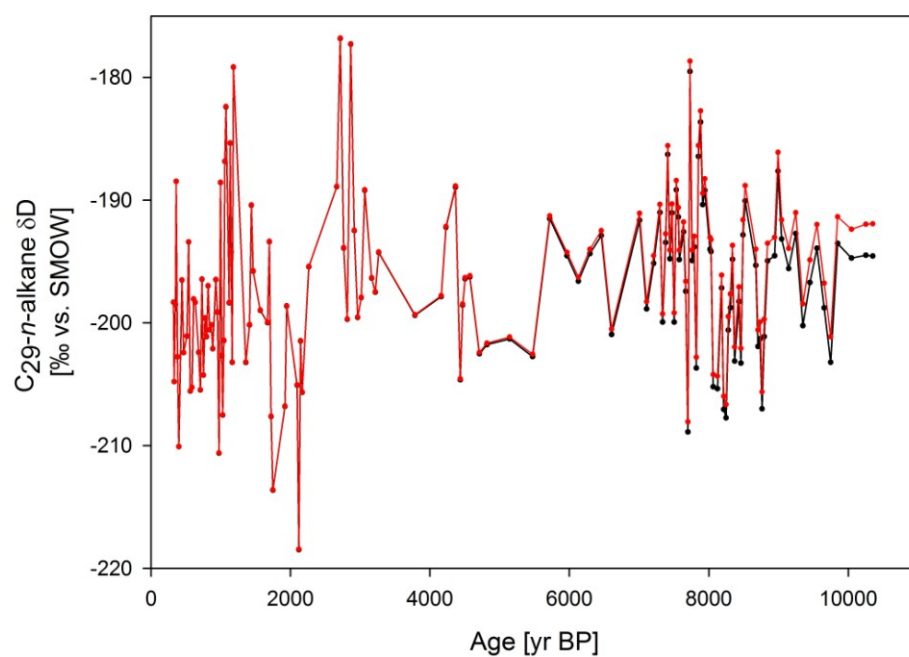


**Figure 3:** δD values of the C<sub>29</sub>-n-alkane (black line and dots) and ice volume corrected δD values of the C<sub>29</sub>-n-alkane (red line and dots).

1296

1297



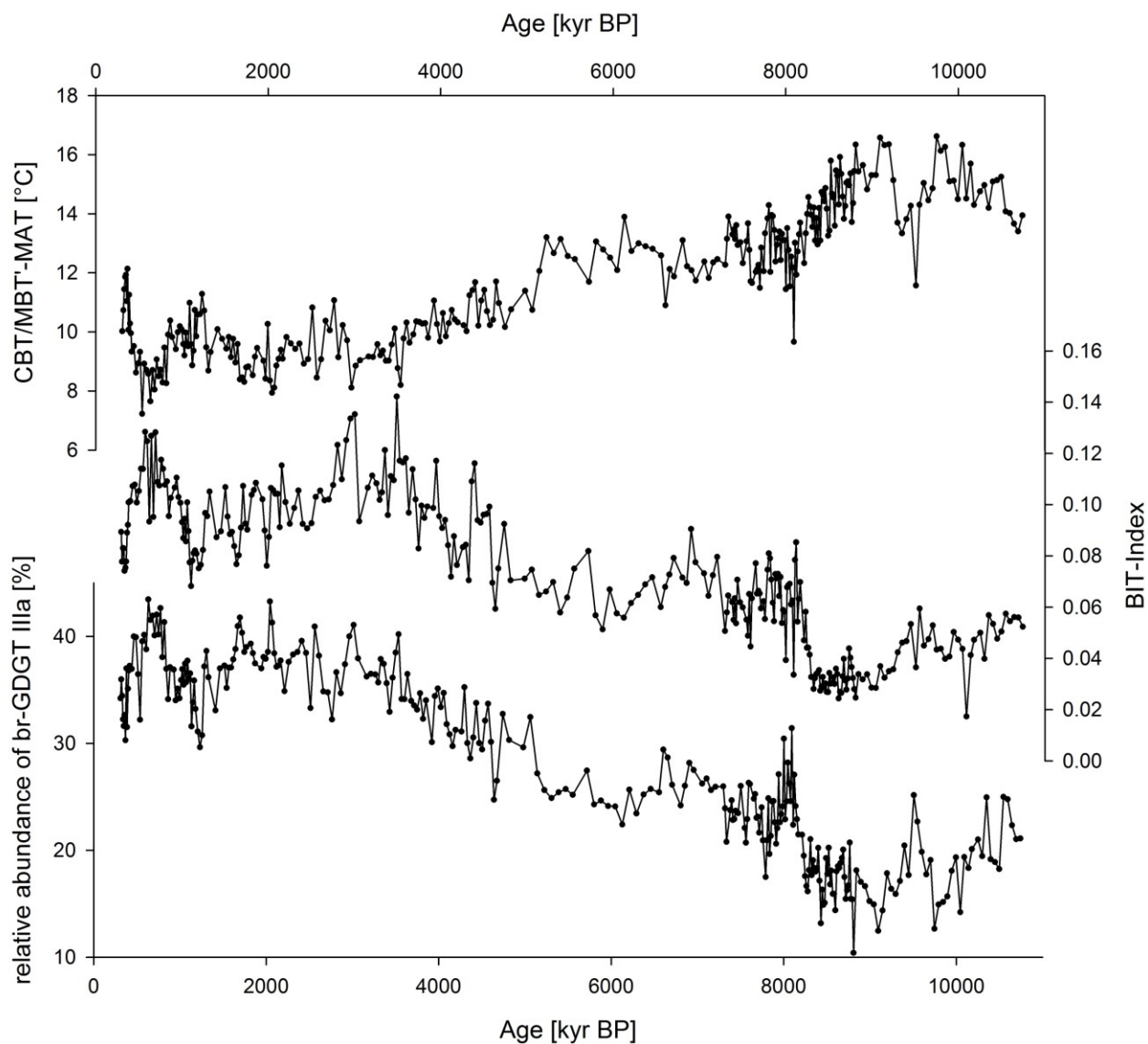


**Figure 4:** Temporal variability of the relative abundance of br-GDGT IIIa related to changes of the BIT-index (Moossen et al., 2013), and the CBT/MBT-MAT reconstructions of Ísafjarðardjúp fjord.

1298

1299

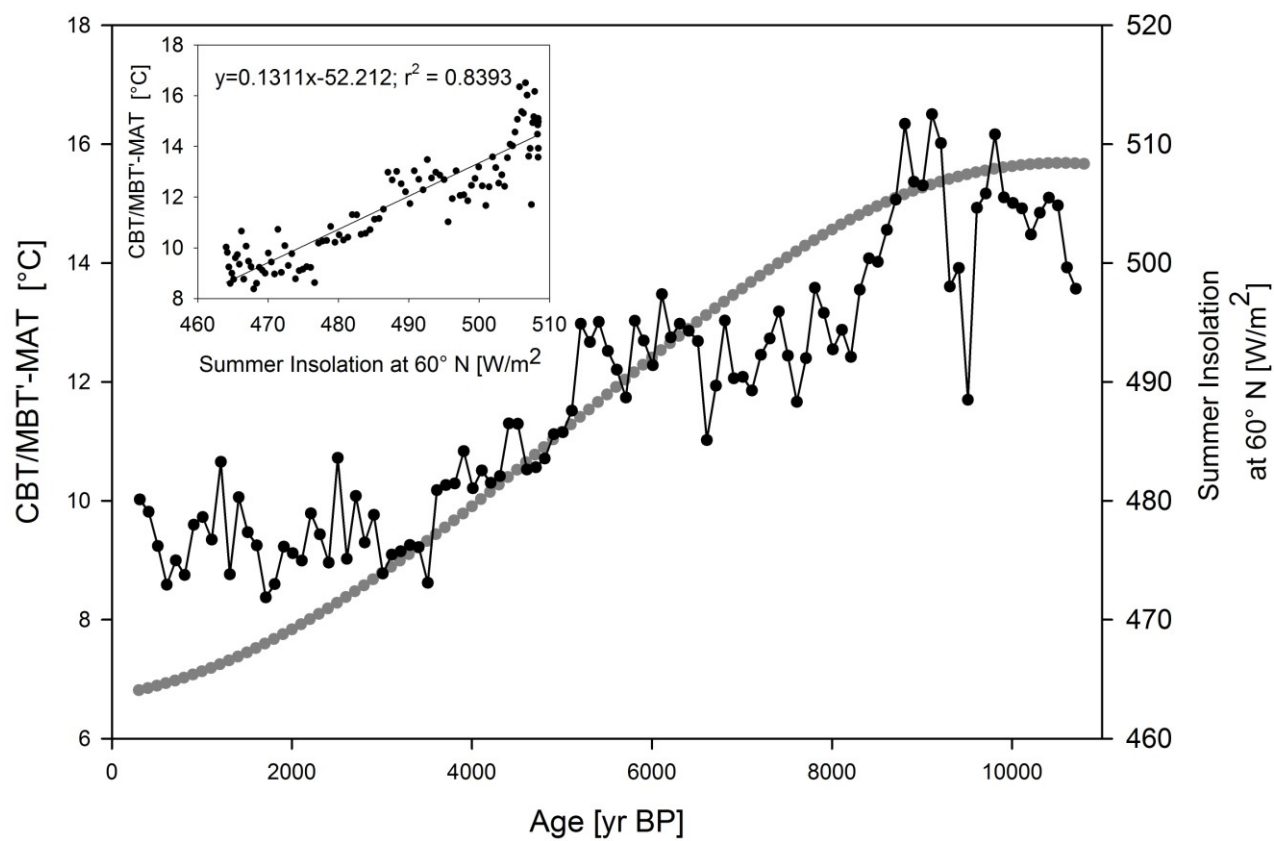


**Figure 5:** Regularly interpolated (sample interval = 100 years) CBT/MBT'-MATs (black dots and line) vs. summer insolation change (grey dots and line; sample interval = 100 years; Laskar et al., 2004). Inset: Linear correlation between CBT/MBT'-MAT and summer insolation.

1300

1301

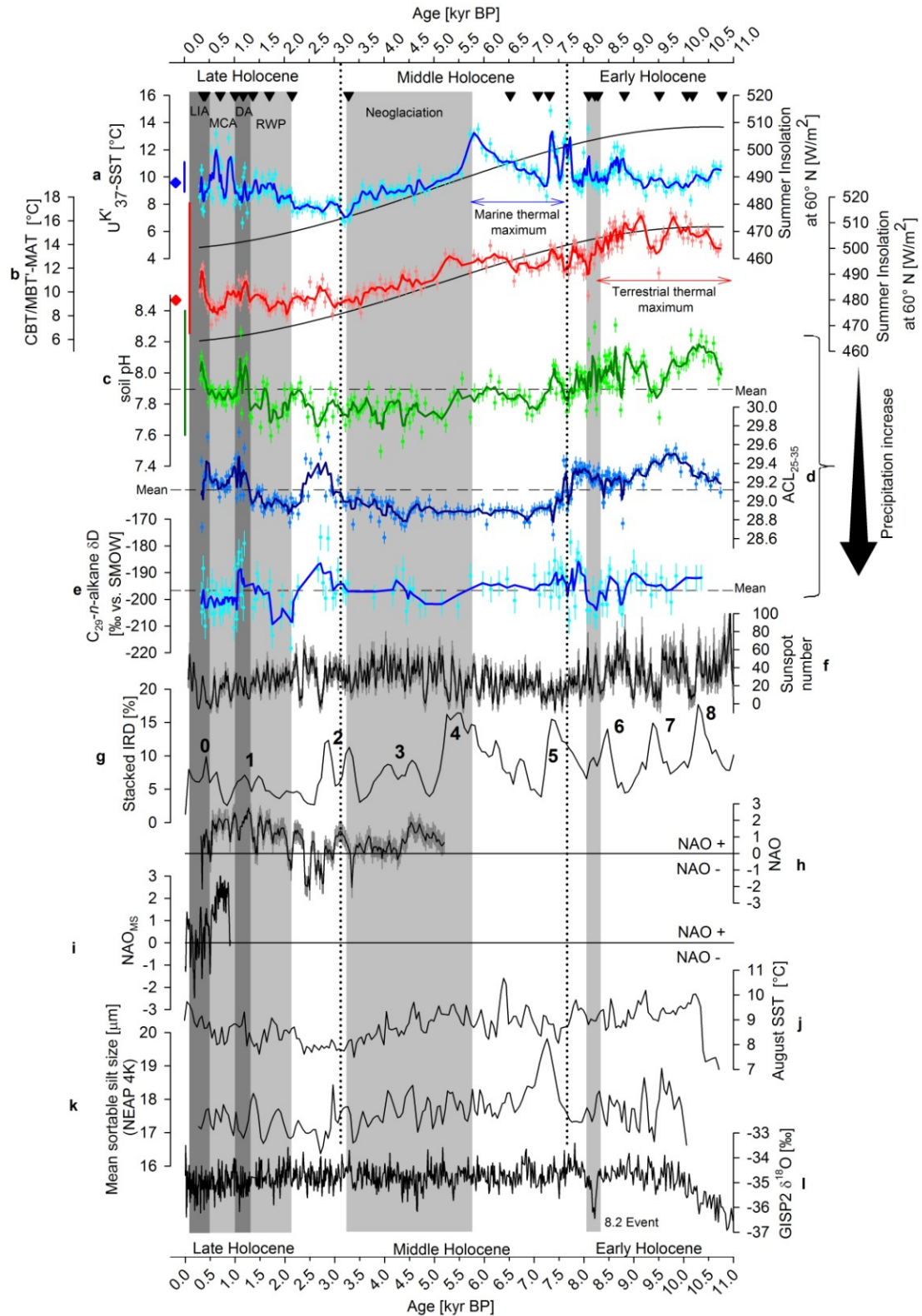


**Figure 6:** Iceland climate records compared with other North Atlantic paleoclimatic records. The LIA, MCA, DA (Dark Ages), RWP (Roman Warm Period), neoglaciation, and the 8.2 ka event are highlighted in shades of grey. The dotted horizontal lines indicate the division from early to middle, and from middle to late Holocene at 7.8 and 3.2 kyr BP. **(a)** alkenone derived  $U^K_{37}$ -SSTs. Raw data and  $1\sigma$  SD (light blue) overlain by the 3-point moving average (dark blue), plotted against summer

insolation change (black line). The vertical blue bar indicates the uncertainty of the calibration equation (1.1 °C; Conte et al., 2006), the blue diamond indicates mean instrumental JJA SSTs at Stykkishólmur (Hanna et al., 2006). Black triangles indicate the  $^{14}\text{C}$ -AMS dated horizons of MD99-2266. **(b)** br-GDGT derived CBT/MBT'-MAT. Raw data and  $1\sigma$  SD (light red) overlaid by the 3-point moving (dark red) is plotted against summer insolation (black line). The vertical red bar indicates the uncertainty of the calibration equation (5.0 °C; Peterse et al., 2012). The red diamond indicates mean instrumental JJA air temperatures at Stykkishólmur (Hanna et al., 2004). **(c)** br-GDGT derived soil pH reconstruction. Raw data and  $1\sigma$  SD (light green) overlain by the 3-point moving average (dark green). The vertical green bar indicates the uncertainty of the calibration equation (Root mean square error: 0.8; Peterse et al., 2012). **(d)** Average chain length variability of leaf wax derived *n*-alkanes ( $\text{ACL}_{25-35}$ ) reconstructing precipitation variability. Raw data and  $1\sigma$  SD (blue) overlain by the 3-point moving average (dark blue). **(e)**  $\delta\text{D}_{\text{C}_{29}}$  reconstructing precipitation change. Raw data and  $1\sigma$  SD (cyan) overlain by the 3-point moving average (blue). The dashed horizontal lines (c-e) indicate the mean Holocene precipitation as indicated by the respective records. **(f)** Holocene sunspot record (Solanki et al., 2004). **(g)** Stacked ice rafted debris (IRD) record revealing numbered Bond-cycles (Bond et al., 2001). **(h)** NAO variability after Olsen et al. (2012). **(i)** NAO variability after Trouet et al. (2009). **(j)** August SSTs on the North Icelandic Shelf after Justwan et al. (2008). **(k)** Mean sortable silt size of the Iceland-Scotland-Overflow-Waters (ISOW) south of Iceland after Hall et al. (2004). **(l)** GISP 2  $\delta^{18}\text{O}$  inferred temperature variations of the North Atlantic area after Grootes and Stuiver (1997).

1302

1303

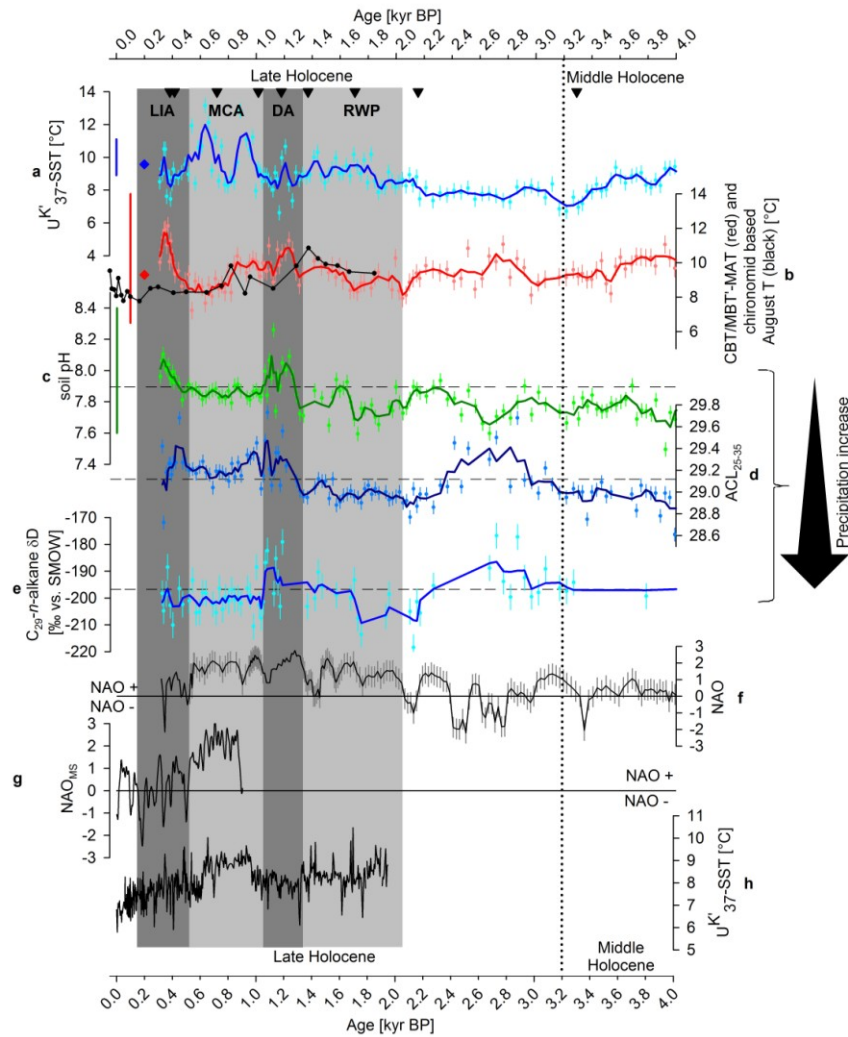


**Figure 7:** Iceland climate records of the youngest 4 kyr BP. The LIA, the MCA, the DA, and the RWP are highlighted in shades of grey. The dotted horizontal line indicates the transition from the middle to the late Holocene. **(a)**  $U^K_{37}$ -SST, raw data and analytical error ( $1\sigma$  SD) is shown in light blue overlain by the 3-point moving average in dark blue. The vertical blue bar indicates the uncertainty of the calibration equation ( $1.1^\circ\text{C}$ ; Conte et al., 2006). The blue diamond indicates mean instrumental JJA SSTs at Stykkishólmur (Hanna et al., 2006). Black triangles indicate the  $^{14}\text{C}$ -AMS dated horizons of MD99-2266. **(b)** CBT/MBT-MAT raw data and analytical error ( $1\sigma$  SD) (light red) overlain by the 3-point moving average (dark red). The vertical red bar indicates the uncertainty of the calibration equation ( $5.0^\circ\text{C}$ ; Peterse et al., 2012). The red diamond indicates mean instrumental JJA air temperatures at Stykkishólmur (Hanna et al., 2004). The black line and data points shows chironomide based August SSTs from north Iceland (Axford et al., 2009). **(c)** soil pH reconstruction raw data and analytical error ( $1\sigma$  SD; light green) overlain by 3-point moving average (dark green). The vertical green bar indicates the uncertainty of the calibration equation ( $0.8$ ; Peterse et al., 2012). **(d)** Average chain length variability of leaf wax derived  $n$ -alkanes ( $ACL_{25-35}$ ) raw data and analytical error ( $1\sigma$  SD; blue) overlain by the 3-point moving average (dark blue). **(e)**  $\delta D_{C_{29}}$  raw data and analytical error ( $1\sigma$  SD; cyan) overlain by the 3-point moving average (blue). The dashed horizontal lines (c-e) indicate the mean Holocene precipitation as indicated by the respective records. **(f)** NAO variability after Olsen et al. (2012). **(g)** NAO variability after Trouet et al. (2009). **(h)**  $U^K_{37}$ -SST reconstruction from the North Icelandic Shelf (Sicre et al., 2011).

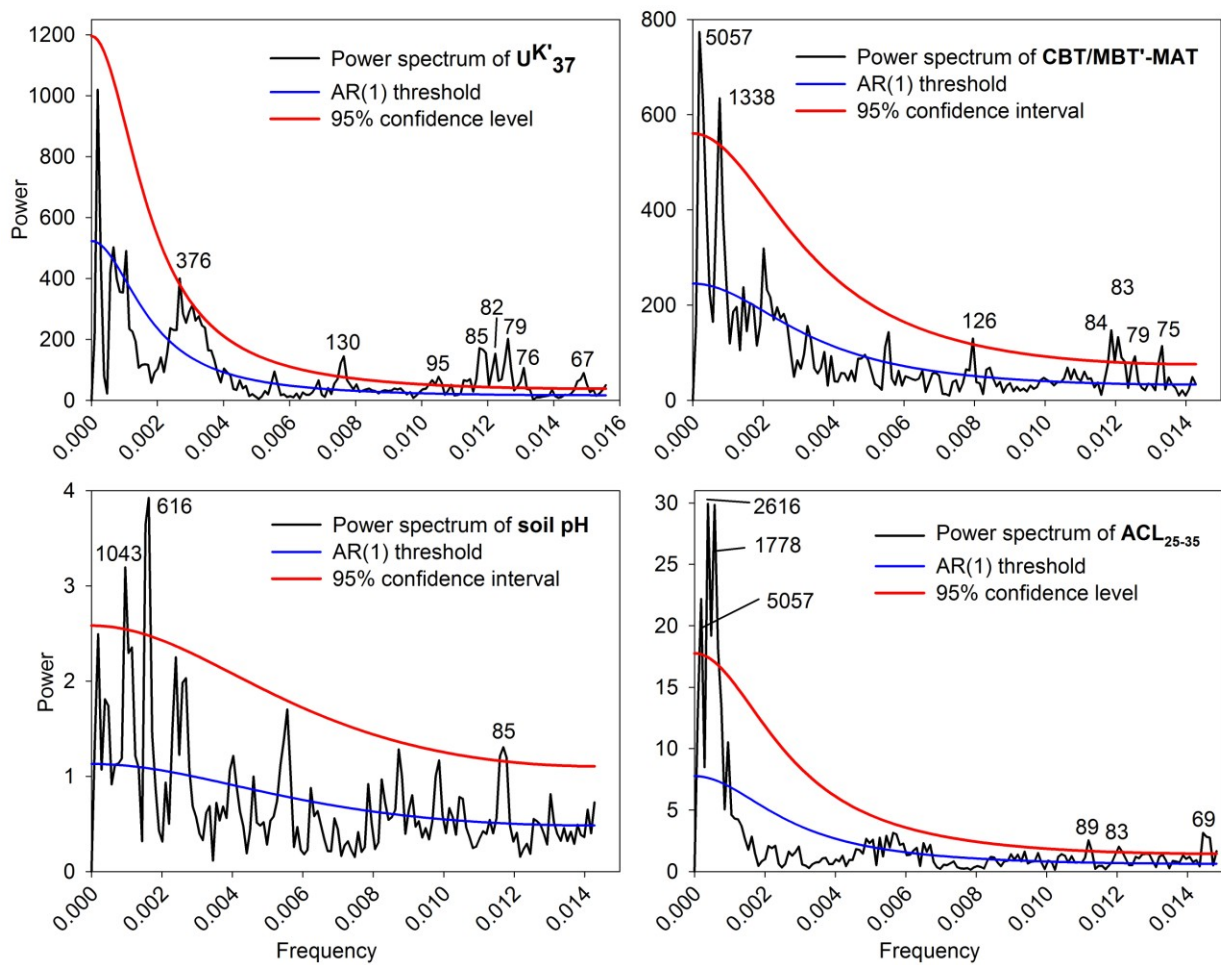


**Figure 8:** REDFIT power spectra of the  $U^{K'}_{37}$ -SST, CBT/MBT'-MAT, soil pH and  $ACL_{25-35}$  time series. The blue line delimits the AR(1) red noise model threshold. The red line indicates the 95 % confidence interval. The periodicities (years) of significant spectral peaks is indicated in each spectrum.